

A comprehensive numerical study on four categories of holographic dark energy models

Jun-Xian Li,^a Shuang Wang,^{1a}

^aSchool of Physics and Astronomy, Sun Yat-Sen University, Zhuhai, China

E-mail: lijx389@mail2.sysu.edu.cn, wangshuang@mail.sysu.edu.cn

Abstract. Holographic dark energy (HDE), which arises from a theoretical attempt of applying the holographic principle (HP) to the dark energy (DE) problem, has attracted significant attention over the past two decades. We perform a most comprehensive numerical study on HDE models that can be classified into four categories: 1) HDE models with other characteristic length scale, 2) HDE models with extended Hubble scale, 3) HDE models with dark sector interaction, 4) HDE models with modified black hole entropy. For theoretical models, we select seven representative models, including the original HDE (OHDE) model, Ricci HDE (RDE) model, generalized Ricci HDE (GRDE) model, interacting HDE (IHDE1 and IHDE2) models, Tsallis HDE (THDE) model, and Barrow HDE (BHDE) model. For cosmological data, we use the Baryon Acoustic Oscillation (BAO) data from the Dark Energy Spectroscopic Instrument (DESI) 2024 measurements, the Cosmic Microwave Background (CMB) distance priors data from the Planck 2018, and the type Ia supernovae (SNe) data from the PantheonPlus compilation. Using χ^2 statistic and Bayesian evidence, we compare these HDE models with current observational data. It is found that: 1) The Λ CDM remains the most competitive model, while the RDE model is ruled out. 2) HDE models with dark sector interaction perform the worst across the four categories, indicating that the interaction term is not favored under the framework of HDE. 3) The other three categories show comparable performance. The OHDE model performs better in the BAO+CMB dataset, and the HDE models with modified black hole entropy perform better in the BAO+CMB+SN dataset. 4) HDE models with the future event horizon exhibit significant discrepancies in parameter space across datasets. The BAO+CMB dataset favors a phantom-like HDE, whereas the BAO+CMB+SN leads to an equation of state (EoS) much closer to the cosmological constant.

ArXiv ePrint: [2412.09064](https://arxiv.org/abs/2412.09064)

¹Corresponding author.

Contents

1	Introduction	1
2	Data and Methodology	3
2.1	Data	3
2.1.1	Baryon Acoustic Oscillation	3
2.1.2	Cosmic Microwave Background	5
2.1.3	Type Ia Supernovae	5
2.2	Methodology	6
2.2.1	chi-squared χ^2 statistic	6
2.2.2	Bayesian evidence	7
3	Holographic Dark Energy Models and Cosmology-Fits Results	8
3.1	Fiducial model	8
3.2	HDE models with other characteristic length scale	9
3.2.1	original holographic dark energy (OHDE) model	9
3.3	HDE models with extended Hubble scale	11
3.3.1	Ricci dark energy (RDE) model	11
3.3.2	Generalized Ricci dark energy (GRDE) model	13
3.4	HDE models with dark sector interaction	13
3.4.1	Interacting holographic dark energy (IHDE) model with Hubble horizon	14
3.4.2	Interacting holographic dark energy (IHDE) model with future event horizon	15
3.5	HDE models with modified black hole entropy	17
3.5.1	Tsallis holographic dark energy (THDE) with Hubble horizon	17
3.5.2	Barrow holographic dark energy (BHDE) model with future event horizon	18
4	Conclusion	20
5	Summary	22

1 Introduction

In 1988, observations of Type Ia supernovae led to the groundbreaking discovery of cosmic acceleration, revealing the existence of a mysterious dominant component: dark energy (DE) [1, 2]. The Λ Cold Dark Matter (Λ CDM) model, which interprets DE as a cosmological constant, has been widely regarded as the standard model of modern cosmology. However, the Λ CDM model still faces some theoretical challenges, such as the fine-tuning problem and the coincidence problem [3–16]. Moreover, in terms of observation, the Λ CDM model faces the “Hubble tension” problem, a discrepancy between the directly measured current cosmic expansion rate and its inferred value from early-universe observations [17–25].

Recently, the Λ CDM model has encountered a new observational challenge. The DESI collaboration released its first-year data on BAO [26]. By analyzing the observational data with the Chevallier-Polarski-Linder (CPL) parameterization [27], the DESI collaboration found the sign of time-varying DE EoS. Initially, this sign was observed with a significance

of 2.6σ in a combined analysis of DESI BAO and CMB data. After including various SNe Ia datasets, the discrepancy intensified, with a significance ranging from 2.5σ to 3.9σ . Because of these theoretical and observational challenges to the Λ CDM model, it is necessary to explore dynamical DE models [28, 29].

Dynamical DE models suggest that the Universe’s accelerated expansion is driven by a time-evolving DE, characterized by an EoS $w(z)$ that varies with redshift z . Notable dynamical DE models had been proposed, such as quintessence [30, 31], phantom [32], k-essence [33–35], Chaplygin gas [36–38], etc. For a comprehensive overview of recent developments in this area, we refer the reader to Refs. [39–45].

As a prominent example of dynamical DE, HDE originates from a theoretical attempt of applying the holographic principle (HP) [46, 47] to the DE problem. The HP states that all the information contained within a volume of space can be encoded on the boundary of that space, much like a hologram. It means that the energy density of DE ρ_{de} can also be described by quantities on the boundary of the universe, including the characteristic length scale L and the reduced Planck mass $M_P^2 \equiv 1/(8\pi G)$. Based on the dimensional analysis, we have [48]:

$$\rho_{de} = C_1 M_P^4 + C_2 M_P^2 L^{-2} + C_3 L^{-4} + \dots, \quad (1.1)$$

where C_1, C_2, C_3 are constant parameters. However, the leading term is 10^{120} times larger than the cosmological observations [5], so this term should be excluded. Moreover, compared with the second term, the third term and the other terms are negligible and can be disregarded. Therefore, the expression of ρ_{de} can be written as [48]:

$$\rho_{de} = 3C^2 M_P^2 L^{-2}, \quad (1.2)$$

where C is a dimensionless constant parameter. It is important to emphasize that Eq. (1.2) serves as the foundational expression for the HDE energy density.

Theoretically, HDE exhibits a strong dependence on the choice of characteristic length scale L . Although the Hubble scale $L = 1/H$ is a natural choice for the characteristic length scale, it has been demonstrated that this choice leads to an incorrect EoS for DE [49–51]. Over the past two decades, extensive studies on HDE had led to various theoretical models. These models can be divided into four main categories [52]: (1)HDE model with other characteristic length scale [53–57]; (2)HDE models with extended Hubble scale [58–61]; (3)HDE models with dark sector interaction [62–66]; (4)HDE models with modified black hole entropy [67–73].

On the other hand, the numerical studies of various HDE models had also attracted considerable attention [74–104]. It should be emphasized that, previous studies mainly focused on the individual HDE models. For examples, Ref. [105] investigated the cosmological constraints on the OHDE model, and found that it performs a litter better than the Λ CDM model for the combined datasets including Planck CMB angular and weak lensing power spectra, Atacama Cosmology Telescope temperature power spectra, BAO, redshift-space distortion (RSD) and Cepheids-Supernovae measurement from SH0ES team (R22). However, after adding the PantheonPlus SN data, it was found that the advantages of OHDE relative to Λ CDM diminish. Ref. [106] found that the OHDE and the interacting HDE models are statistically as viable as the Λ CDM model for the combined datasets of DESI BAO and SN data, but these HDE models become less favored after the CMB data are included. Ref. [107] investigated the entropy-based approaches to HDE and the corresponding Gravity-Thermodynamics (GT) formalisms, and found that the HDE approach is statisti-

Model Category	Model	Reference
HDE models with other characteristic length scale	OHDE	[53]
HDE models with extended Hubble scale	RDE GRDE	[59] [60]
HDE models with dark sector interaction	IHDE1 IHDE2	[62] [63]
HDE models with modified black hole entropy	THDE BHDE	[67] [70]

Table 1. HDE models and their references.

cally equivalent to the Λ CDM model for the combined datasets of PantheonPlus, DESy5, and DESI BAO.

In this paper, instead of studying an individual HDE model, we perform a most comprehensive numerical study on all the four categories of HDE models. Specifically, we select one or two representative models from each category, as summarized in Table 1. For the first category, we discuss the OHDE model. For the second category, we analyze both the RDE and GRDE models. For the third category, we examine two interacting HDE models (IHDE1 and IHDE2), one with the Hubble scale as the IR cutoff and the other with the future event horizon as IR cutoff. For the fourth category, we consider the THDE and BHDE models. We also consider the Λ CDM model as the fiducial model. For observational data, we adopt the BAO data from DESI 2024 DR1, the CMB distance priors data from Planck 2018, and the SN Ia data from PantheonPlus compilation. To perform numerical analysis, we divide these observational data into two datasets: the first dataset only includes DESI BAO and Planck 2018 CMB data, while the second dataset combines the first dataset with the PantheonPlus SN data. Moreover, we apply the χ^2 statistic to perform cosmology-fits, and then calculate the Bayesian evidence of these HDE models to compare their relative performance.

The paper is organized as follows: In Section 2, we outline the data and the methodology used in our analysis. In Section 3, we introduce seven representative HDE models and present their joint observational constraints. In Section 4, we draw conclusions based on observational constraints. Section 5 provides a brief summary.

2 Data and Methodology

2.1 Data

2.1.1 Baryon Acoustic Oscillation

For the BAO data, we adopt the first-year data released by the DESI collaboration [26], which includes observations from four different classes of extragalactic targets: the bright galaxy sample (BGS) [108], luminous red galaxies (LRG) [109], emission line galaxies (ELG) [110], and quasars (QSO) [111]. Table 2 presents the tracers, effective redshifts, observables, and measurement values for the seven BAO data points.

The quantities of BAO listed in Table 2 correspond to several key distances: D_M , D_H , and D_V . In a spatially flat FLRW universe, the transverse comoving distance D_M at redshift z is defined as [26]:

$$D_M(z) = \frac{c}{H_0} \int_0^z \frac{dz'}{H(z')/H_0}, \quad (2.1)$$

Tracer	z_{eff}	D_M/r_d	D_H/r_d	r or D_V/r_d
BGS	0.295	—	—	7.93 ± 0.15
LRG1	0.510	13.62 ± 0.25	20.98 ± 0.61	-0.445
LRG2	0.706	16.85 ± 0.32	20.08 ± 0.60	-0.420
LRG3+ELG1	0.930	21.71 ± 0.28	17.88 ± 0.35	-0.389
ELG2	1.317	27.79 ± 0.69	13.82 ± 0.42	-0.444
QSO	1.491	—	—	26.07 ± 0.67
Lya QSO	2.330	39.71 ± 0.94	8.52 ± 0.17	-0.477

Table 2. Statistics from the DESI DR1 BAO measurements. Note that for each sample DESI DR1 measures either both D_M/r_d and D_H/r_d , which are correlated with a coefficient r , or D_V/r_d .

where c is the speed of light, $H_0 = 100h \text{ km s}^{-1}\text{Mpc}^{-1}$ with h the dimensionless Hubble constant. The distance variable D_H is related to the Hubble parameter $H(z)$ as $D_H(z) = c/H(z)$. The angle-averaged distance D_V is given by $D_V(z) = [zD_M(z)^2D_H(z)]^{1/3}$.

In Table 2, BAO measurements depend on the radius of the sound horizon at the drag epoch r_d . This represents the distance that sound can travel between the Big Bang and the drag epoch, which marks the time when baryons decoupled. The sound horizon can be expressed as [26]:

$$r_s(z) = \int_z^\infty \frac{c_s(z')}{H(z')} dz', \quad (2.2)$$

where $c_s(z)$ is the speed of sound which, prior to recombination, is given by

$$c_s(z) = \frac{c}{\sqrt{3 \left(1 + \frac{3\rho_b}{4\rho_r}\right)}} \quad (2.3)$$

where ρ_b and ρ_r are the baryon and radiation densities, respectively. Specifically, $\bar{R}_b/(1+z) = 3\rho_b/(4\rho_r)$, and $\bar{R}_b = 31500\Omega_b h^2 (T_{\text{CMB}}/2.7\text{K})^{-4}$, where Ω_b is the fractional density of baryons. The radiation term in the $H(z)$ can be determined by the matter-radiation equality relation $\Omega_r = \Omega_m/(1+z_{eq})$, and $z_{eq} = 2.5 \times 10^4 \Omega_m h^2 (T_{\text{CMB}}/2.7\text{K})^{-4}$. Here, Ω_r and Ω_m are the fractional densities of radiation and matter, respectively. We assume the CMB temperature to be $T_{\text{CMB}} = 2.7255\text{K}$.

In practice, the redshift of the drag epoch, z_d , is approximated by [112]:

$$z_d = \frac{1291(\Omega_m h^2)^{0.251}}{1 + 0.659(\Omega_m h^2)^{0.828}} [1 + b_1(\Omega_b h^2)^{b_2}], \quad (2.4)$$

$$b_1 = 0.313(\Omega_m h^2)^{-0.419} [1 + 0.607(\Omega_m h^2)^{0.674}], \quad (2.5)$$

$$b_2 = 0.238(\Omega_m h^2)^{0.223}. \quad (2.6)$$

Hence, the sound horizon at the drag epoch is $r_d = r_s(z_d)$. The data vector D can be constructed as

$$D \equiv \begin{pmatrix} D_M/r_d \\ D_H/r_d \end{pmatrix}, \quad (2.7)$$

with its covariance matrix defined as [113]:

$$\text{Cov}_{BAO} = \begin{bmatrix} \sigma_1^2 & r \cdot \sigma_1 \cdot \sigma_2 \\ r \cdot \sigma_1 \cdot \sigma_2 & \sigma_2^2 \end{bmatrix}, \quad (2.8)$$

where σ_1 and σ_2 denote the standard deviations of D_M/r_d and D_H/r_d , respectively. The correlation coefficient between D_M/r_d and D_M/r_d , denoted as r , is provided in Table 2.

2.1.2 Cosmic Microwave Background

For the CMB data, we use the distance priors from Planck 2018 release [114]. The method of distance priors [115–119] serves as a compressed dataset that encapsulates key information from the full CMB data. This approach allows us to substitute the full CMB power spectrum with a more compact representation while retaining key cosmological information.

The distance priors contain two primary features of the CMB power spectrum: the shift parameter R and the acoustic scale l_a . The shift parameter R affects the peak heights in the CMB temperature power spectrum along the line of sight, while the acoustic scale l_a influences the spacing of the peaks in the transverse direction. These parameters are defined as

$$R \equiv \frac{D_M(z_*)\sqrt{\Omega_m H_0^2}}{c}, \quad (2.9)$$

$$l_a \equiv \frac{\pi D_M(z_*)}{r_s(z_*)}, \quad (2.10)$$

where z_* is the redshift at the photon decoupling epoch, which can be calculated by an approximate formula [120]:

$$z_* = 1048[1 + 0.00124(\Omega_b h^2)^{-0.738}][1 + g_1(\Omega_m h^2)^{g_2}], \quad (2.11)$$

where

$$g_1 = \frac{0.0783(\Omega_b h^2)^{-0.238}}{1 + 39.5(\Omega_b h^2)^{0.763}}, \quad (2.12)$$

$$g_2 = \frac{0.560}{1 + 21.1(\Omega_b h^2)^{1.81}}. \quad (2.13)$$

The data vector and its covariance matrix are the following respectively [121]:

$$V^{data} \equiv \begin{pmatrix} R \\ l_a \\ \Omega_b h^2 \end{pmatrix} = \begin{pmatrix} 1.74963 \\ 301.80845 \\ 0.02237 \end{pmatrix}, \quad (2.14)$$

$$\text{Cov}_{CMB} = 10^{-8} \times \begin{bmatrix} 1598.9554 & 17112.007 & -36.311179 \\ 17112.007 & 811208.45 & -494.79813 \\ -36.311179 & -494.79813 & 2.1242182 \end{bmatrix}. \quad (2.15)$$

2.1.3 Type Ia Supernovae

For the SN data, we use a subset of the PantheonPlus compilation [122], consisting of 1701 data points. We remove all SN with $z < 0.01$, as these data points are influenced by model-dependent peculiar velocities that need to be considered separately. This cut leaves us with 1590 data points, spanning a redshift range $0.01016 \leq z \leq 2.26137$. The covariance matrix, Cov_{SN} , includes both statistical and systematic errors.

The theoretical distance modulus μ in a flat universe is given by

$$\mu_{th} = 5 \log_{10} \left[\frac{d_L(z_{hel}, z_{cmb})}{\text{Mpc}} \right] + 25, \quad (2.16)$$

where z_{hel} and z_{cmb} are the heliocentric and CMB rest-frame redshifts of SN. The luminosity distance d_L is

$$d_L(z_{hel}, z_{cmb}) = (1 + z_{hel})r(z_{cmb}), \quad (2.17)$$

where $r(z)$ is the comoving distance given by Eq. (2.1). The observation of distance modulus μ is given by the following empirical linear relation:

$$\mu_{obs} = m_B - M_B + \alpha X_1 - \beta \mathcal{C} - \delta_{bias} + \delta_{host}, \quad (2.18)$$

where m_B is the observed peak magnitude in the rest-frame of the B band, M_B is the fiducial magnitude of a SN, X_1 describes the time stretching of light-curve, and \mathcal{C} describes the supernova color at maximum brightness, δ_{bias} is a correction term to account for selection biases, and δ_{host} is the luminosity correction for residual correlations. Note that α and β are global nuisance parameters relating stretch and color, respectively.

2.2 Methodology

2.2.1 chi-squared χ^2 statistic

The χ^2 statistic quantifies the goodness of fit between predicted values from cosmological models and actual measurements from astronomical observations. By minimizing the χ^2 function, one can identify the model parameters that best describe the observed universe.

There are two methods to calculate the χ^2 function. For independent data points, the χ^2 function is defined as

$$\chi_\xi^2 = \frac{(\xi_{th} - \xi_{obs})^2}{\sigma_\xi^2}, \quad (2.19)$$

where ξ_{th} is the theoretically predicted value, ξ_{obs} is the experimentally measured value, and σ_ξ is the standard deviation. For correlated data points, the χ^2 function is given by

$$\chi^2 = \Delta\xi^T \text{Cov}^{-1} \Delta\xi, \quad (2.20)$$

where $\Delta\xi \equiv \xi_{th} - \xi_{obs}$, and Cov is a covariance matrix that characterizes the errors in the data.

For **BAO data**, the χ^2 function is split into two parts:

$$\chi_{BAO}^2 = \chi_1^2 + \chi_2^2, \quad (2.21)$$

where χ_1^2 represents the data D_V/r_d from tracer BGS and QSO, and is expressed as

$$\chi_1^2 = \sum_i \frac{(\xi_i^{th} - \xi_i^{data})^2}{\sigma_i^2}. \quad (2.22)$$

The second term, χ_2^2 , represents the data for D_M/r_d and D_H/r_d from tracers LRG1, LRG2, LRG3+ELG1, ELG2, and Ly α QSO, and is expressed as

$$\chi_2^2 = \sum_i \Delta D_i^T \text{Cov}_{BAO}^{-1} \Delta D_i, \quad (2.23)$$

where $\Delta D_i = D_i^{th} - D_i^{data}$ is the data vector constructed by Eq. (2.7).

For **CMB data**, the χ^2 function for the CMB distance priors can be expressed as

$$\chi_{CMB}^2 = \Delta V^T \text{Cov}_{CMB}^{-1} \Delta V, \quad (2.24)$$

where $\Delta V = V^{th} - V^{data}$ is the data vector constructed by Eq. (2.14).

For **SN data**, the χ^2 can be calculated as

$$\chi_{SN}^2 = \Delta\mu^T \cdot \text{Cov}_{SN}^{-1} \cdot \Delta\mu, \quad (2.25)$$

where $\Delta\mu \equiv \mu_{th} - \mu_{obs}$ is the data vector, and Cov_{SN}^{-1} is the inverse matrix of the total covariance matrix provided by the Supernova Collaboration [122].

Since we use the BAO data from DESI DR1, the CMB data from Planck 2018 distance priors, and the SN data from PantheonPlus, the total χ^2 is

$$\chi^2 = \chi_{BAO}^2 + \chi_{CMB}^2 + \chi_{SN}^2. \quad (2.26)$$

In this work, we sample from the dark energy parameter posterior distributions using the MCMC code **Cobaya** [123] with the **mcmc** sampler [124, 125]. Convergence of an MCMC run is assessed using the Gelman-Rubin statistic [126] with a tolerance of $|R - 1| < 0.01$. We analyze the MCMC chains using **Getdist** [127] to visualize the contour plots for the resulting posterior distributions.

2.2.2 Bayesian evidence

Bayesian evidence, also known as the marginal likelihood, plays a pivotal role in model selection and parameter estimation within the Bayesian framework. Specifically, it quantifies how well a model fits the data by integrating the prior distribution of the model parameters with the likelihood function. Here, we use the **PolyChord** sampler [128, 129], a nested sampler incorporated in **Cobaya**, to compute the Bayesian evidence for our models.

Given some dataset \mathcal{D} , a model \mathcal{M} with parameter θ can be used to calculate the likelihood $\mathcal{L}_{\mathcal{M}}(\theta) \equiv P(\mathcal{D}|\theta, \mathcal{M})$. By applying Bayes' theorem, this can be inverted to determine the posterior distribution of the parameters:

$$P(\theta|\mathcal{D}, \mathcal{M}) \equiv \mathcal{P}_{\mathcal{M}}(\theta) = \frac{\mathcal{L}_{\mathcal{M}}(\theta)\pi_{\mathcal{M}}(\theta)}{\mathcal{Z}_{\mathcal{M}}}, \quad (2.27)$$

where $\pi_{\mathcal{M}}(\theta) \equiv P(\theta|\mathcal{M})$ is the prior degree of belief on the values of the parameters and $\mathcal{Z}_{\mathcal{M}} \equiv P(\mathcal{D}|\mathcal{M})$ is the evidence or marginal likelihood, calculated as

$$\mathcal{Z}_{\mathcal{M}} = \int \mathcal{L}_{\mathcal{M}}(\theta)\pi_{\mathcal{M}}(\theta)d\theta. \quad (2.28)$$

The evidence can be neglected in model fitting, but it becomes crucial in model comparison.

When comparing two different models, \mathcal{M}_1 and \mathcal{M}_2 , the ratio of their posterior probabilities, P_1 and P_2 , is proportional to the ratio of their evidence. This relationship can be expressed as

$$\frac{P_1(\theta_1|\mathcal{D}, \mathcal{M}_1)}{P_2(\theta_2|\mathcal{D}, \mathcal{M}_2)} = \frac{\pi_{\mathcal{M}_1}(\theta_1)\mathcal{Z}_{\mathcal{M}_1}}{\pi_{\mathcal{M}_2}(\theta_2)\mathcal{Z}_{\mathcal{M}_2}}. \quad (2.29)$$

This ratio between posteriors leads to the definition of the Bayes Factor B_{12} , which in logarithmic scale is written as

$$\ln \mathcal{B}_{12} \equiv \log \left[\frac{\mathcal{Z}_{\mathcal{M}_1}}{\mathcal{Z}_{\mathcal{M}_2}} \right] = \ln[\mathcal{Z}_{\mathcal{M}_1}] - \ln[\mathcal{Z}_{\mathcal{M}_2}]. \quad (2.30)$$

If $\ln \mathcal{B}_{12}$ is larger (smaller) than unity, the data favors model \mathcal{M}_1 (\mathcal{M}_2). In our analysis, we take the Λ CDM as the reference model \mathcal{M}_2 .

3 Holographic Dark Energy Models and Cosmology-Fits Results

Following the description of the data and methods, we now present the fiducial model and the seven HDE models, along with the corresponding cosmology-fits results.

3.1 Fiducial model

We adopt the Λ CDM model as the fiducial model. The Friedmann equation of this model can be expressed as

$$E(z) \equiv \frac{H(z)}{H_0} = \sqrt{\Omega_r(1+z)^4 + \Omega_m(1+z)^3 + \Omega_{de}}, \quad (3.1)$$

where $\Omega_{de} = 1 - \Omega_r - \Omega_m$.

Fig. 1 presents the one-dimensional posterior distributions and two-dimensional marginalized contours of combined observational constraints for the Λ CDM model. The red contours represents constraints from the DESI BAO + CMB, while the blue contours represents constraints from the DESI BAO + CMB + PantheonPlus. Both datasets give similar results, showing good compatibility. The best-fit values for the parameters are listed in Table 3.

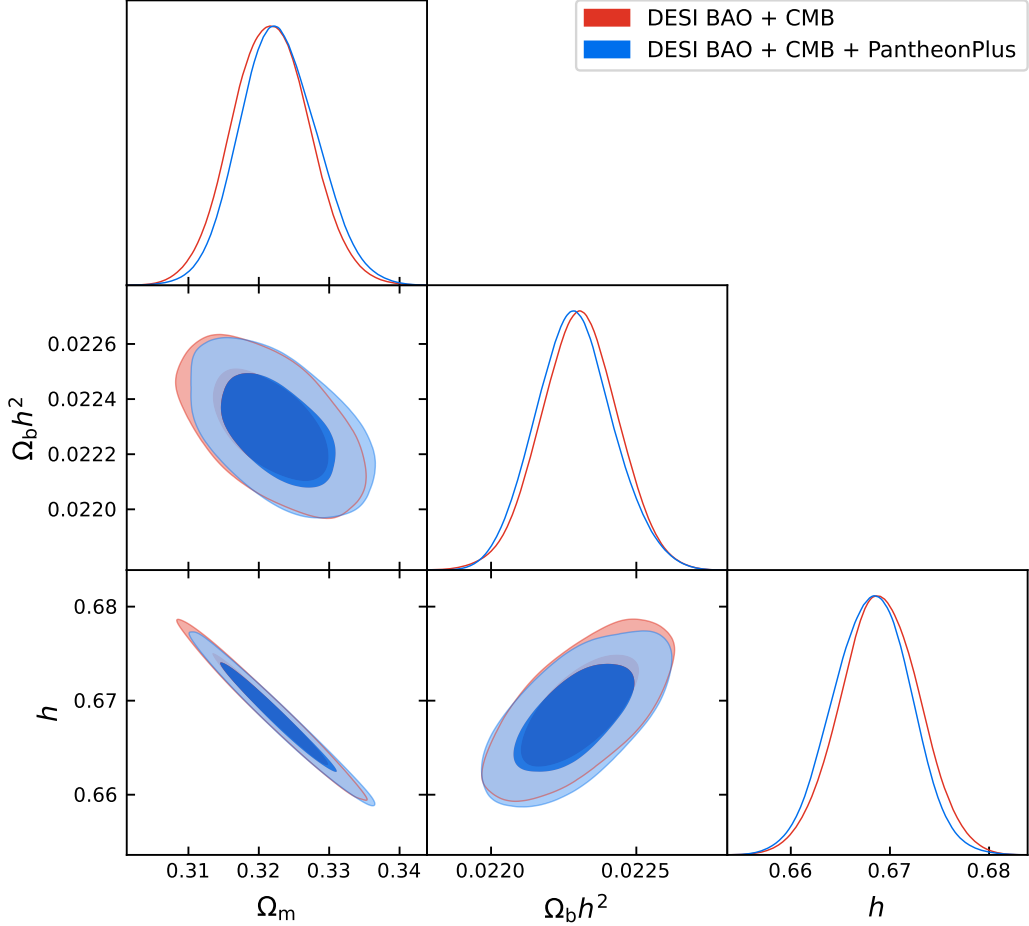


Figure 1. One-dimensional posterior distributions and two-dimensional marginalized contours at 1σ and 2σ levels for Λ CDM model

DESI BAO + CMB					
Model	Ω_m	$\Omega_b h^2$	h	Parameter 1	Parameter 2
Λ CDM	$0.3218^{+0.0098}_{-0.0100}$	$0.02230^{+0.00025}_{-0.00024}$	$0.6689^{+0.0074}_{-0.0070}$	-	-
OHDE	$0.2802^{+0.0348}_{-0.0358}$	$0.02238^{+0.00028}_{-0.00030}$	$0.7143^{+0.0533}_{-0.0423}$	$C = 0.5287^{+0.1131}_{-0.0934}$	-
RDE	$0.1376^{+0.0101}_{-0.0021}$	$0.02276^{+0.00035}_{-0.00030}$	$0.9995^{+0.0004}_{-0.0351}$	$\alpha = 0.1911^{+0.0083}_{-0.0069}$	-
GRDE	$0.2991^{+0.0381}_{-0.0436}$	$0.02235^{+0.00036}_{-0.00031}$	$0.6915^{+0.0563}_{-0.0416}$	$\lambda = 0.8539^{+0.1820}_{-0.1466}$	$\beta = 0.5543^{+0.1299}_{-0.1034}$
IHDE1	$0.3497^{+0.0156}_{-0.0128}$	$0.02240^{+0.0003}_{-0.0003}$	$0.6392^{+0.0122}_{-0.0131}$	$\varepsilon = 1.8465^{+0.0618}_{-0.0533}$	-
IHDE2	$0.2710^{+0.0487}_{-0.0438}$	$0.02239^{+0.00033}_{-0.00034}$	$0.7263^{+0.0686}_{-0.0587}$	$b^2 = -0.0018^{+0.0020}_{-0.0019}$	$C = 0.4913^{+0.1845}_{-0.1124}$
THDE	$0.3200^{+0.0237}_{-0.0245}$	$0.02228^{+0.00030}_{-0.00029}$	$0.6710^{+0.0281}_{-0.0245}$	$\delta = 2.0211^{+0.2430}_{-0.1732}$	-
BHDE	$0.2921^{+0.0321}_{-0.0338}$	$0.02236^{+0.00028}_{-0.00030}$	$0.7000^{+0.0459}_{-0.0361}$	$\Delta = 0.2349^{+0.0740}_{-0.0724}$	-
DESI BAO + CMB + PantheonPlus					
Model	Ω_m	$\Omega_b h^2$	h	Parameter 1	Parameter 2
Λ CDM	$0.3221^{+0.0103}_{-0.0094}$	$0.02229^{+0.00024}_{-0.00024}$	$0.6686^{+0.0067}_{-0.0072}$	-	-
OHDE	$0.3283^{+0.0154}_{-0.0141}$	$0.02246^{+0.00030}_{-0.00028}$	$0.6570^{+0.0134}_{-0.0142}$	$C = 0.6929^{+0.0664}_{-0.0521}$	-
RDE	$0.3434^{+0.0158}_{-0.0152}$	$0.02325^{+0.00030}_{-0.00029}$	$0.6196^{+0.0125}_{-0.0123}$	$\alpha = 0.3003^{+0.0097}_{-0.0092}$	-
GRDE	$0.3264^{+0.0159}_{-0.0170}$	$0.02236^{+0.00035}_{-0.00033}$	$0.6618^{+0.0181}_{-0.0154}$	$\lambda = 0.9907^{+0.0757}_{-0.0775}$	$\beta = 0.6518^{+0.0565}_{-0.0612}$
IHDE1	$0.3451^{+0.0128}_{-0.0123}$	$0.02241^{+0.00031}_{-0.00031}$	$0.6433^{+0.0114}_{-0.0117}$	$\varepsilon = 1.8282^{+0.0530}_{-0.0473}$	-
IHDE2	$0.3279^{+0.0167}_{-0.0165}$	$0.02239^{+0.00034}_{-0.00033}$	$0.6596^{+0.0174}_{-0.0157}$	$b^2 = -0.0002^{+0.0017}_{-0.0017}$	$C = 0.7171^{+0.0867}_{-0.0704}$
THDE	$0.3233^{+0.0164}_{-0.0138}$	$0.02231^{+0.00029}_{-0.00029}$	$0.6666^{+0.0153}_{-0.0151}$	$\delta = 1.9818^{+0.1261}_{-0.1047}$	-
BHDE	$0.3261^{+0.0157}_{-0.0137}$	$0.02241^{+0.00030}_{-0.00027}$	$0.6606^{+0.0130}_{-0.0147}$	$\Delta = 0.1581^{+0.0298}_{-0.0379}$	-

Table 3. Best-fit values with 1σ confidence level (CL) for model parameters obtained from constraints using DESI BAO + CMB and DESI BAO + CMB + PantheonPlus datasets.

3.2 HDE models with other characteristic length scale

3.2.1 original holographic dark energy (OHDE) model

In the OHDE model [53], an accelerating expanding universe is achieved by choosing the future event horizon as the characteristic length, defined as

$$L = a \int_t^\infty \frac{dt'}{a} = a \int_a^\infty \frac{da'}{H a'^2}, \quad (3.2)$$

where a is the scale factor $a = (1+z)^{-1}$. In this case, the Friedmann equation reads

$$3M_P^2 H^2 = \rho_r + \rho_m + \rho_{de}, \quad (3.3)$$

or equivalently,

$$E(z) = \sqrt{\frac{\Omega_r(1+z)^4 + \Omega_m(1+z)^3}{1 - \Omega_{de}(z)}}. \quad (3.4)$$

With conservation equation

$$\dot{\rho}_{de} + 3H\rho_{de}(1+w) = 0, \quad (3.5)$$

and taking derivative for Eq. (1.2) with respect to $x \equiv \ln a$, the EoS is given by

$$w = -\frac{1}{3} - \frac{2\sqrt{\Omega_{de}}}{3C}. \quad (3.6)$$

It is obvious that the EoS of the OHDE evolves dynamically and satisfies $-(1 + 2/C)/3 \leq w \leq -1/3$ due to $0 \leq \Omega_{de} \leq 1$. Taking derivative of Ω_{de} as well, the dynamical evolution equation of $\Omega_{de}(z)$ is obtained as

$$\frac{d\Omega_{de}(z)}{dz} = -\frac{2\Omega_{de}(z)(1 - \Omega_{de}(z))}{1+z} \left(\frac{1}{2} + \frac{\sqrt{\Omega_{de}(z)}}{C} + \frac{\Omega_r(z)}{2(1 - \Omega_{de}(z))} \right). \quad (3.7)$$

Solving Eq. (3.7) numerically and substituting the corresponding results into Eq. (3.4), one can obtain the redshift evolution of Hubble parameter $H(z)$ of the OHDE model, enabling cosmological constraints to be obtained.

Fig. 2 presents the one-dimensional posterior distributions and two-dimensional marginalized contours of combined observational constraints for the OHDE model. While the BAO+CMB (red) data alone provides a broad constraint, the inclusion of PantheonPlus data (blue) generally tightens the parameter constraints, particularly for Ω_m , C , and h . The blue contours favor higher values of Ω_m and C , and lower value of h . In addition, there is a noticeable discrepancy between the results for the blue contours and those for the red contours.

The best-fit values derived from the sample likelihood constraints are listed in Table 3. For the BAO+CMB dataset, the best-fit values with 1σ confidence level (CL) are $\Omega_m = 0.2802^{+0.0348}_{-0.0358}$, $h = 0.7143^{+0.0533}_{-0.0423}$, and $C = 0.5287^{+0.1131}_{-0.0934}$, which yields the EoS of $w = -1.40^{+0.21}_{-0.26}$. In contrast, for the BAO+CMB+SN dataset, we have $\Omega_m = 0.3283^{+0.0154}_{-0.0141}$, $h = 0.6570^{+0.0134}_{-0.0142}$, $C = 0.6929^{+0.0664}_{-0.0521}$, resulting in $w = -1.12^{+0.07}_{-0.07}$. Based on the parameter constrain results given by the two datasets, the discrepancies¹ for Ω_m , C , and h are 1.25σ , 1.29σ , and 1.15σ , respectively. The issue of parameter discrepancies has been discussed in previous literature. In Ref. [130], the authors also found a parameter discrepancy when constraining the OHDE model using two datasets, BAO+CMB and BAO+CMB+SN, with BAO data from SDSS, CMB data from Planck 2018, and SN data from Pantheon. This discrepancy arises due to the presence of a turning point in $E(z)$.

Both datasets (BAO+CMB and BAO+CMB+SN) give a EoS of HDE $w < -1$, implying that the OHDE has phantom-like characteristics. Moreover, only taking into account the BAO+CMB dataset, the EoS of the OHDE deviates significantly from the cosmological constant (i.e. $w = -1$). On the contrary, the inclusion of PantheonPlus SN data leads to the EoS of the OHDE being much closer to the cosmological constant. This implies that under the framework of HDE with future event horizon as the IR cutoff, the PantheonPlus dataset does not favor a dynamical DE.

¹Given the central values μ_X and μ_Y of quantities X and Y , along with their asymmetric uncertainties σ_{X+} , σ_{X-} , and σ_{Y+} , σ_{Y-} , the sigma deviation is calculated as: Sigma deviation = $\Delta\mu/\sqrt{\sigma_X^2 + \sigma_Y^2}$, where $\Delta\mu = |\mu_X - \mu_Y|$, $\sigma_i^2 = (\sigma_{i+} + \sigma_{i-})/2$.

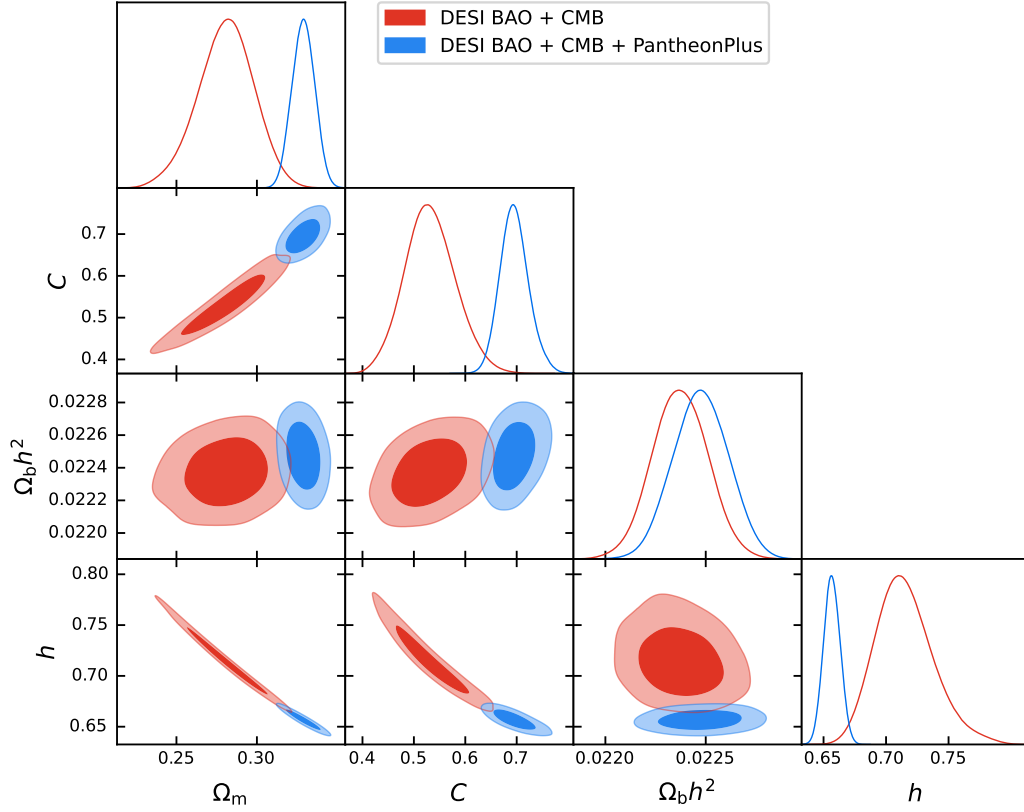


Figure 2. One-dimensional posterior distributions and two-dimensional marginalized contours at 1σ and 2σ levels for OHDE model.

3.3 HDE models with extended Hubble scale

In these HDE models, IR cutoff is identified with combination of Hubble parameter and its time derivative.

3.3.1 Ricci dark energy (RDE) model

The Ricci dark energy (RDE) model [59] is a representative model to describe DE by using the Ricci scalar curvature as the IR cutoff. In a flat universe, the Ricci scalar curvature is given by

$$R = -6(2H^2 + \dot{H}), \quad (3.8)$$

where the dot represents the derivative with respect to time. Taking the Ricci scalar curvature as the IR cutoff, the energy density of RDE can be expressed as

$$\rho_{de} = 3\alpha M_P^2(2H^2 + \dot{H}), \quad (3.9)$$

where α is a constant to be determined. The Friedmann equation for this model is

$$H^2 = \frac{1}{3M_P^2}(\rho_m e^{-3x} + \rho_r e^{-4x}) + \alpha \left(2H^2 + \frac{1}{2} \frac{dH^2}{dx} \right). \quad (3.10)$$

Solving this equation and applying the initial condition $E_0 = E(t_0) = 1$ lead to the scaled Hubble expansion rate as

$$E^2(z) = \Omega_r(1+z)^4 + \Omega_m(1+z)^3 + \frac{\alpha}{2-\alpha}\Omega_m(1+z)^3 + \left(1 - \Omega_r - \frac{2\Omega_m}{2-\alpha}\right)(1+z)^{4-\frac{2}{\alpha}}. \quad (3.11)$$

Fig. 3 presents the one-dimensional posterior distributions and two-dimensional marginalized contours of combined observational constraints for the RDE model. This model has very poor performance. Significant discrepancies are observed in the parameter constraints between two datasets. In particular, the contours for BAO+CMB dataset exceed the specified prior ranges, indicating a substantial mismatch between the model predictions and the observational data. The poor performance of the RDE model, which is consistent with previous studies [87, 88], can be attributed to its violation of the null energy condition [130]. Therefore, the RDE model is ruled out by observational data.

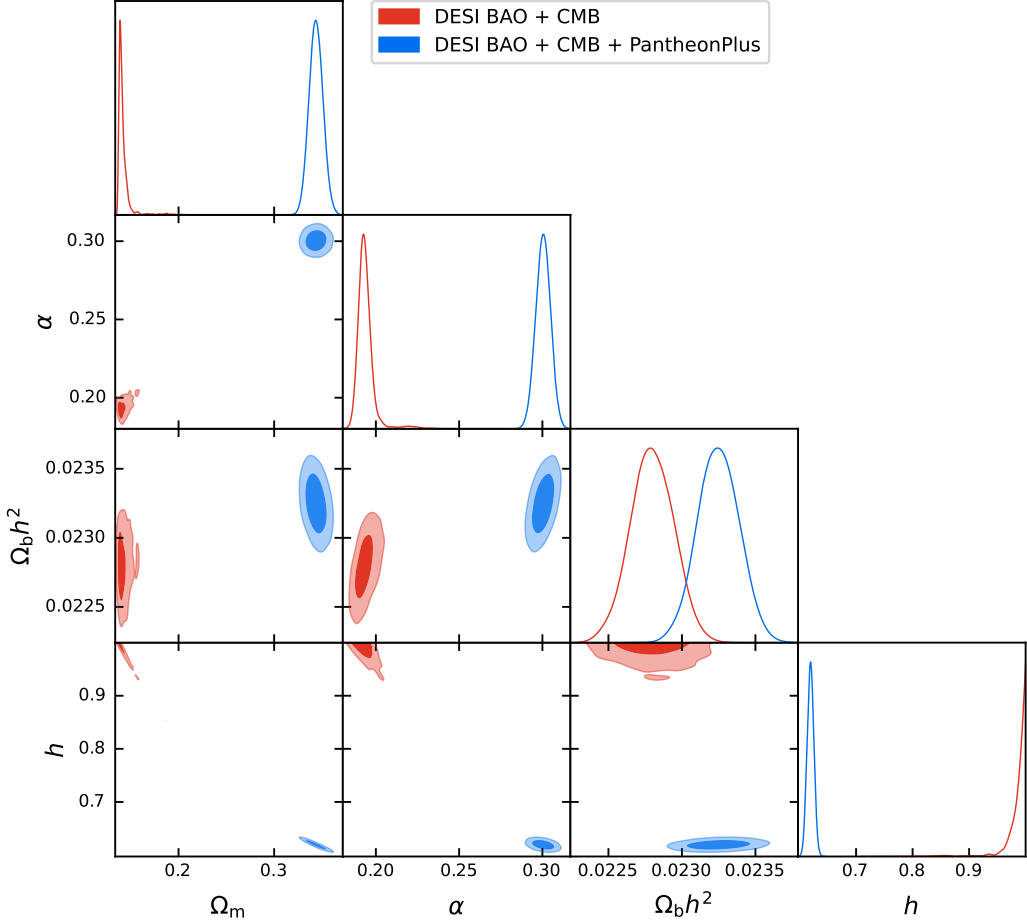


Figure 3. One-dimensional posterior distributions and two-dimensional marginalized contours at 1σ and 2σ levels for RDE model

3.3.2 Generalized Ricci dark energy (GRDE) model

Granda and Oliveros proposed a generalization of the Ricci scalar as the IR cutoff in HDE models [60]. In this model, the cutoff is expressed as

$$L^{-2} = \lambda H^2 + \beta \dot{H}, \quad (3.12)$$

where λ and β are independent model parameters. This cutoff is commonly known as the Granda-Oliver (GO) cutoff. Since the model takes a generalized Ricci scalar as the cutoff, we refer to it as the GRDE model. The corresponding holographic dark energy density is given by

$$\rho_{de} = 3M_P^2(\lambda H^2 + \beta \dot{H}). \quad (3.13)$$

The Friedmann equation for this model is

$$\begin{aligned} E(z)^2 = & \Omega_r(1+z)^4 + \Omega_m(1+z)^3 + \frac{2\beta - \lambda}{\lambda - 2\beta - 1} \Omega_r(1+z)^4 \\ & + \frac{3\beta - 2\lambda}{2\lambda - 3\beta - 2} \Omega_m(1+z)^3 + f_0(1+z)^{2(\lambda-1)/\beta}, \end{aligned} \quad (3.14)$$

where the last three terms give the scale dark energy density Ω_{de} , f_0 can be determined by initial condition $E_0 = E(t_0) = 1$ as

$$f_0 = 1 - \frac{2\Omega_m}{3\beta - 2\alpha + 2} - \frac{\Omega_r}{2\beta - \alpha + 1}. \quad (3.15)$$

With conservation equation, the EoS is given by

$$w = \frac{2(\lambda - 1) + (2 - 3\beta)\Omega_m + (2 - 4\beta)\Omega_r}{3\beta(1 - \Omega_m - \Omega_r)} - 1. \quad (3.16)$$

Fig. 4 presents the one-dimensional posterior distributions and two-dimensional marginalized contours of combined observational constraints for the GRDE model. The red and blue contours are generally compatible, with minor shifts observed in parameter distributions when PantheonPlus data is added. Specifically, the addition of SN data slightly tightens constraints on parameters such as Ω_m , λ , β , and h , as reflected in the narrower blue contours. A noticeable correlation between λ and β persists in the BAO+CMB+SN dataset.

The best-fit values derived from the sample likelihood constraints are listed in Table 3. For the BAO+CMB dataset, the best-fit values with 1σ CL are $\Omega_m = 0.2991^{+0.0381}_{-0.0436}$, $h = 0.6915^{+0.0563}_{-0.0416}$, $\lambda = 0.8539^{+0.1820}_{-0.1466}$, and $\beta = 0.5543^{+0.1299}_{-0.1034}$, yielding an EoS of $w = -1.16^{+0.22}_{-0.11}$. In the BAO+CMB+SN dataset, we have $\Omega_m = 0.3264^{+0.0159}_{-0.0170}$, $h = 0.6618^{+0.0181}_{-0.0154}$, $\lambda = 0.9907^{+0.0757}_{-0.0775}$, and $\beta = 0.6518^{+0.0565}_{-0.0612}$, resulting in $w = -1.00^{+0.08}_{-0.06}$, which brings the EoS of the GRDE model closer to that of Λ CDM. Based on the parameter constrain results given by the two datasets, the discrepancies for Ω_m , λ , β , and h are 0.61σ , 0.75σ , 0.74σ , and 0.57σ , respectively.

The BAO+CMB datasets give a EoS of GRDE $w < -1$, corresponding to phantom-like characteristics. On the contrary, the inclusion of PantheonPlus SN data leads to a EoS of GRDE $w = -1$. It shows that the PantheonPlus dataset does not favor a dynamical DE.

3.4 HDE models with dark sector interaction

In these HDE models, dark energy and dark matter no longer evolve independently but interact with each other.

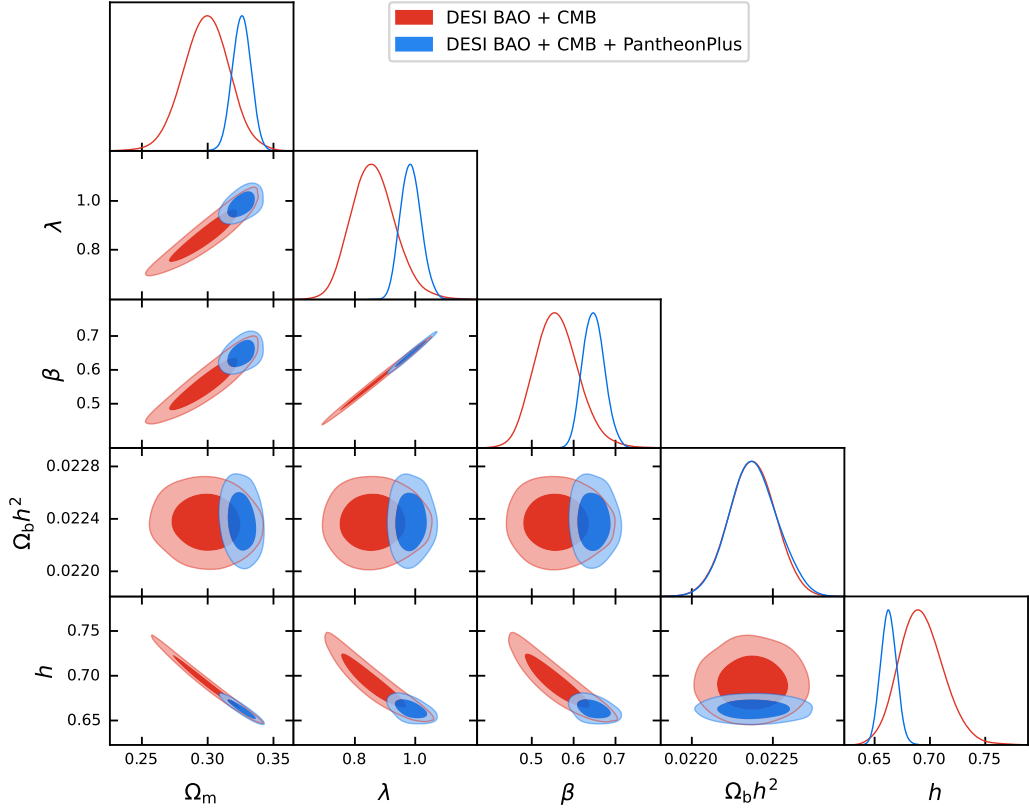


Figure 4. One-dimensional posterior distributions and two-dimensional marginalized contours at 1σ and 2σ levels for GRDE model

3.4.1 Interacting holographic dark energy (IHDE) model with Hubble horizon

Taking into account the mutual interaction, the energy densities of DE and dark matter evolve according to the equations below [131, 132]:

$$\dot{\rho}_m + 3H\rho_m = Q, \quad (3.17)$$

$$\dot{\rho}_{de} + 3H(1+w)\rho_{de} = -Q, \quad (3.18)$$

where Q denotes the interaction term. As shown in [133], the presence of interaction Q enables the Hubble scale to serve as the cutoff length.

By adopting the Hubble scale as the IR cutoff and following the growth assumption in [62], the interaction term is given by

$$Q = 3\eta\rho_m H a^\varepsilon, \quad (3.19)$$

where ε and η are positive-definite parameters. Using the ansatz (3.19), the scaled Hubble rate is expressed as [62]

$$\frac{H(z)}{H_0} = (1+z)^{3/2} \exp \left[\frac{3\eta}{2\varepsilon} ((1+z)^{-\varepsilon} - 1) \right]. \quad (3.20)$$

Comparing Eq. (3.20) with the corresponding quantity of the Λ CDM:

$$\begin{aligned}\frac{H(z)_{\Lambda CDM}}{H_0} &= \sqrt{\frac{\Omega_\Lambda}{\Omega_\Lambda + \Omega_m}} \left[1 + \frac{\Omega_m}{\Omega_\Lambda} (1+z)^3 \right]^{1/2} \\ &= 1 + \frac{3}{2} \frac{\Omega_m}{\Omega_\Lambda + \Omega_m} z + \mathcal{O}(z^2),\end{aligned}\tag{3.21}$$

we obtain the scaled Hubble rate for this IHDE model as follows

$$\begin{aligned}E(z) &= (1+z)^{3/2} \exp \left[\frac{3\eta}{2\varepsilon} ((1+z)^{-\varepsilon} - 1) \right] \\ &= 1 + \frac{3}{2} (1-\eta) z + \mathcal{O}(z^2).\end{aligned}\tag{3.22}$$

As shown in [62], Eq. (3.22) must coincide with Eq. (3.21) up to linear order in z . This requirement allows the parameter η to be determined as

$$\eta = \frac{\Omega_{de}}{\Omega_{de} + \Omega_m}.\tag{3.23}$$

Once η is determined, the scaled Hubble rate can be written as

$$E(z) = (1+z)^{3/2} \exp \left[\frac{3(1-\Omega_m)}{2\varepsilon} ((1+z)^{-\varepsilon} - 1) \right].\tag{3.24}$$

Since this IHDE model adopts the Hubble scale as the IR cutoff, we refer to it as the IHDE1 model.

Fig. 5 presents the one-dimensional posterior distributions and two-dimensional marginalized contours of combined observational constraints for the IHDE1 model. The red contours represents constraints from the DESI BAO + CMB, while the blue contours represents constraints from the DESI BAO + CMB + PantheonPlus. The parameter constraints are consistent across both datasets, with no deviations caused by the inclusion of SN data.

The best-fit values derived from the sample likelihood constraints are listed in Table 3. For the BAO+CMB dataset, the best-fit values with 1σ CL are $\Omega_m = 0.3497^{+0.0156}_{-0.0128}$, $\varepsilon = 1.8465^{+0.0618}_{-0.0533}$, and $h = 0.6392^{+0.0122}_{-0.0131}$. In the BAO+CMB+SN dataset, we have $\Omega_m = 0.3451^{+0.0128}_{-0.0123}$, $\varepsilon = 1.8282^{+0.0530}_{-0.0473}$, and $h = 0.6433^{+0.0114}_{-0.0117}$. Based on the χ^2 statistic and Bayesian evidence results, which will be discussed in the next chapter, it is found that the IHDE1 model is not favored by observational data.

3.4.2 Interacting holographic dark energy (IHDE) model with future event horizon

An alternative approach to the Hubble scale is to use the future event horizon as the IR cutoff. In this model, the interaction term takes the form $Q = 3b^2 M_P^2 H(\rho_{de} + \rho_m)$ with b^2 the coupling constant [63]. By combining the interaction term and energy conservation equations (3.17, 3.18), the evolution equation for $\Omega_{de}(z)$ is written as

$$\frac{d\Omega_{de}}{dz} = -\frac{\Omega_{de}^2}{1+z} (1-\Omega_{de}) \left[\frac{1}{\Omega_{de}} + \frac{2}{C\sqrt{\Omega_{de}}} - \frac{3b^2 - \Omega_r}{\Omega_{de}(1-\Omega_{de})} \right].\tag{3.25}$$

The Friedmann equation in this model satisfies

$$\frac{1}{E(z)} \frac{dE(z)}{dz} = -\frac{\Omega_{de}}{1+z} \left(\frac{1}{2} + \frac{\sqrt{\Omega_{de}}}{C} + \frac{3b^2 - 3 - \Omega_r}{2\Omega_{de}} \right).\tag{3.26}$$

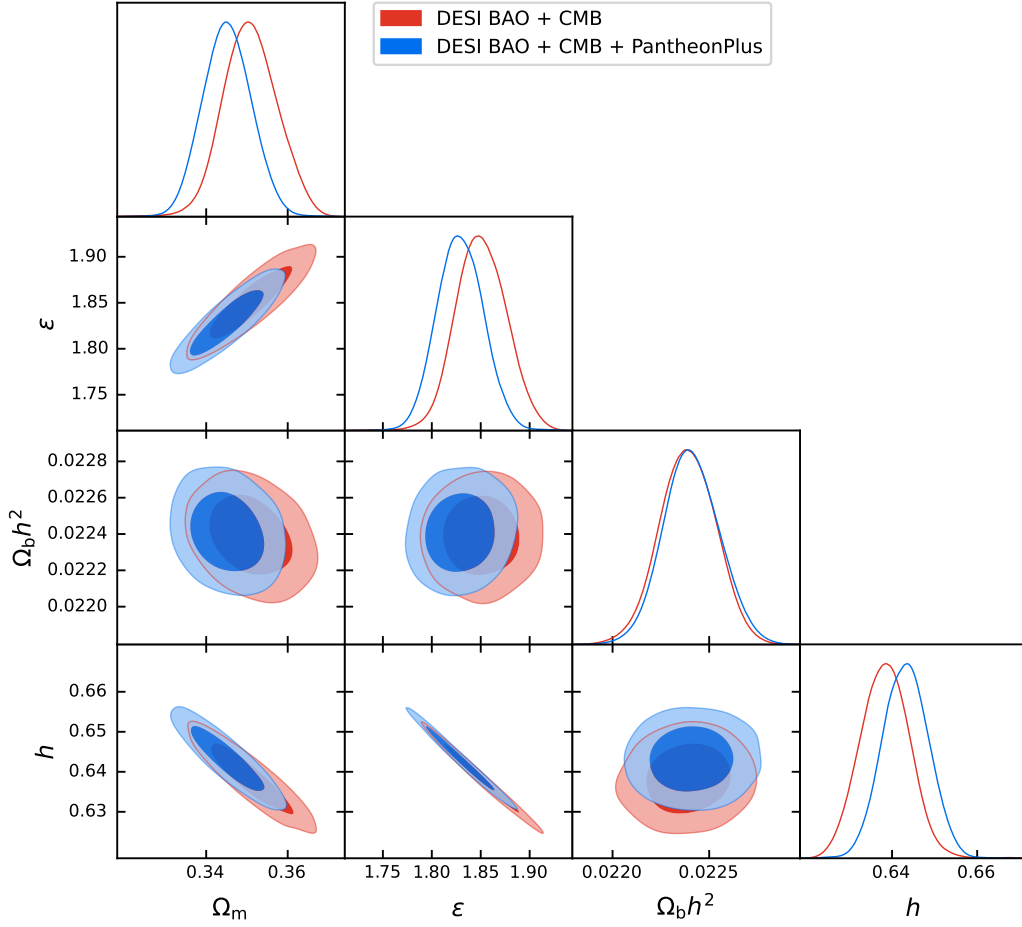


Figure 5. One-dimensional posterior distributions and two-dimensional marginalized contours at 1σ and 2σ levels for IHDE1 model

By numerically solving the above equation, we then obtain the evolutions of both Ω_{de} and $E(z)$ as functions of redshift. The EoS is given by

$$w = -\frac{1}{3} - \frac{2\sqrt{\Omega_{de}}}{3C} - \frac{b^2}{\Omega_{de}}. \quad (3.27)$$

Since this IHDE model adopts the future event horizon as the IR cutoff, we refer to it as the IHDE2 model.

Fig. 6 presents the one-dimensional posterior distributions and two-dimensional marginalized contours of combined observational constraints for the IHDE2 model. The overall constraint patterns show similarities to those observed in the OHDE. While the BAO+CMB (red) data provides a broad constraint, the inclusion of PantheonPlus data (blue) generally tightens the parameter constraints, particularly for Ω_m , b^2 , C , and h . The blue contours favor higher values of Ω_m , b^2 , C , and lower value of h . In addition, there is a noticeable discrepancy between the results for the blue contours and those for the red contours.

The best-fit values derived from the sample likelihood constraints are listed in Table 3. For the BAO+CMB dataset, the best-fit values with 1σ CL are $\Omega_m = 0.2710^{+0.0487}_{-0.0438}$, $h = 0.7263^{+0.0686}_{-0.0587}$, $b^2 = -0.0018^{+0.0020}_{-0.0019}$, and $C = 0.4913^{+0.1845}_{-0.1124}$, which yields the EoS of $w =$

$-1.48^{+0.34}_{-0.39}$. In the BAO+CMB+SN dataset, we have $\Omega_m = 0.3279^{+0.0167}_{-0.0165}$, $h = 0.6596^{+0.0174}_{-0.0157}$, $b^2 = -0.0002^{+0.0017}_{-0.0017}$, and $C = 0.7171^{+0.0867}_{-0.0704}$, resulting in $w = -1.09^{+0.09}_{-0.09}$. Based on the parameter constrain results given by the two datasets, the discrepancies for Ω_m , b^2 , C , and h are 1.15σ , 0.61σ , 1.34σ , and 1.01σ , respectively.

Both two datasets give a EoS $w < -1$, indicating that the IHDE2 model also has the phantom-like characteristics. The best-fit coupling b^2 is very close to zero but remains negative, suggesting a weak interaction with potential energy transfer from the matter to DE. Similar to the OHDE model, the EoS of the IHDE2 model deviates significantly from the Λ CDM case ($w = -1$) when only the BAO+CMB data are taken into account. However, the inclusion of the SN data leads to the EoS of IHDE2 much closer to the cosmological constant. This implies that the PantheonPlus dataset does not favor a dynamical DE.

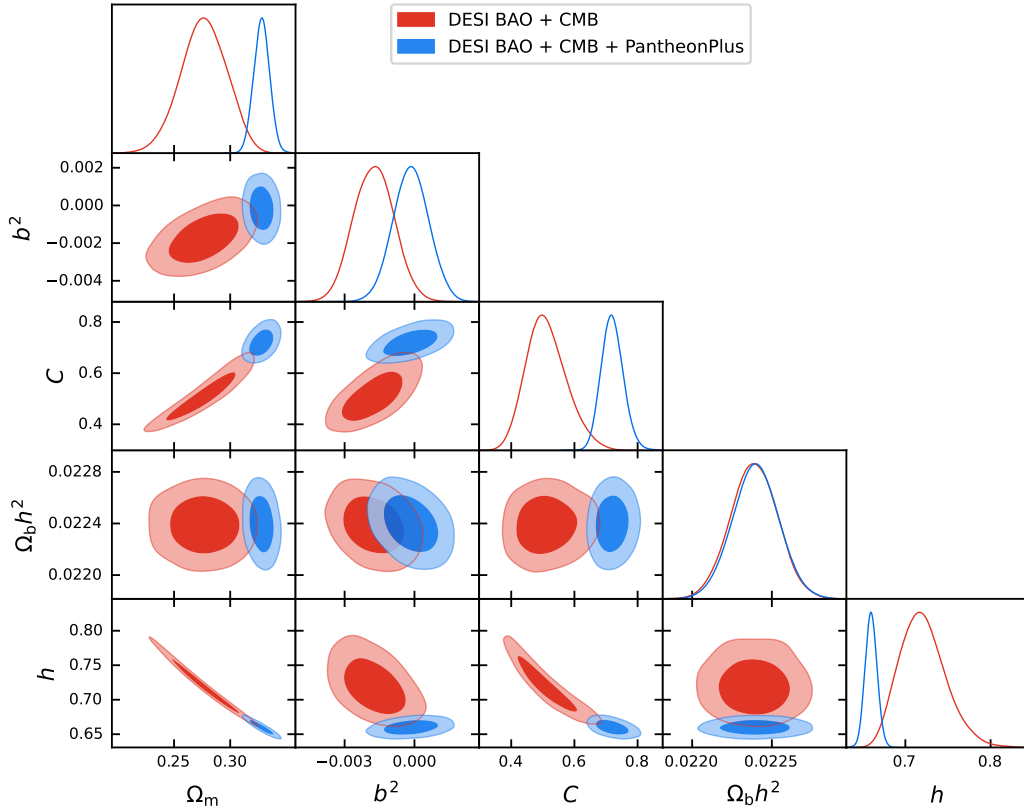


Figure 6. One-dimensional posterior distributions and two-dimensional marginalized contours at 1σ and 2σ levels for IHDE2 model

3.5 HDE models with modified black hole entropy

In these HDE models, the HDE density depends on the specific entropy-area relationship $S \sim A \sim L^2$ of black holes, where $A = 4\pi L^2$ represents the area of the horizon.

3.5.1 Tsallis holographic dark energy (THDE) with Hubble horizon

Tsallis and Cirto proposed that the traditional Boltzmann-Gibbs additive entropy should be generalized to a non-additive entropy, known as Tsallis entropy [134]. This generalized

entropy is given by

$$S_\delta = \gamma A^\delta, \quad (3.28)$$

where γ is an unknown constant, and δ denotes the non-additivity parameter. Building on this concept, M. Tavayef et al. introduced the Tsallis HDE (THDE) model [67]. By substituting the relation (3.28) into the ultraviolet (UV) and IR (L) cutoff $\rho_{de} \leq SL^{-4}$, the energy density of DE is modified as

$$\rho_{de} = BL^{2\delta-4}, \quad (3.29)$$

where $B = 3C^2 M_P^2$. In this model, the Hubble scale is considered a suitable candidate for the IR cutoff, which can lead to the late-time accelerated expansion of the universe. With conservation equation (3.5), the EoS is given by

$$w = \frac{\delta - 1}{(2 - \delta)\Omega_{de} - 1}. \quad (3.30)$$

When $\delta = 2$, the EoS of this model coincides with that of Λ CDM, where $w = -1$. The evolution equation of Ω_{de} is governed by the equation

$$\frac{d\Omega_{de}}{dz} = -\frac{3(\delta - 1)}{1 + z}\Omega_{de} \left(\frac{1 - \Omega_{de} - 5\Omega_r}{1 - (2 - \delta)\Omega_{de}} \right). \quad (3.31)$$

The Friedmann equation of the THDE model satisfies

$$E(z) = \sqrt{\frac{\Omega_r(1+z)^4 + \Omega_m(1+z)^3}{1 - \Omega_{de}(z)}}. \quad (3.32)$$

For our analysis, we fixed $B = 3$ in M_P^2 units to perform constraints. Fig. 7 presents the one-dimensional posterior distributions and two-dimensional marginalized contours of combined observational constraints for the THDE model. The parameter constraints are consistent across both datasets, with no deviations caused by the inclusion of SN data. The addition of SN data slightly tightens constraints on parameters such as Ω_m , δ , and h , as reflected in the narrower blue contours.

The best-fit values derived from the sample likelihood constraints are listed in Table 3. For the BAO+CMB dataset, the best-fit values with 1σ CL are $\Omega_m = 0.3200^{+0.0237}_{-0.0245}$, $h = 0.6710^{+0.0281}_{-0.0245}$, and $\delta = 2.0211^{+0.2430}_{-0.1732}$, which yields the EoS of $w = -1.00^{+0.06}_{-0.05}$. In the BAO+CMB+SN dataset, we have $\Omega_m = 0.3233^{+0.0164}_{-0.0138}$, $h = 0.6666^{+0.0153}_{-0.0151}$, and $\delta = 1.9818^{+0.1261}_{-0.1047}$, resulting in $w = -0.99^{+0.03}_{-0.03}$. The evolution behavior of THDE is very close to Λ CDM.

3.5.2 Barrow holographic dark energy (BHDE) model with future event horizon

In Ref. [135, 136], it was suggested that quantum-gravitational effects may cause deformations on the black hole surface, leading to deviations from the standard Bekenstein-Hawking entropy. This modified entropy, known as Barrow entropy, is expressed as

$$S_B = \left(\frac{A}{A_0} \right)^{1+\Delta/2}, \quad (3.33)$$

where A is the standard horizon area, A_0 is the Planck area, and Δ is a parameter quantifies quantum-gravitational deformation. Here, $0 \leq \Delta \leq 1$, with $\Delta = 0$ corresponding to a smooth

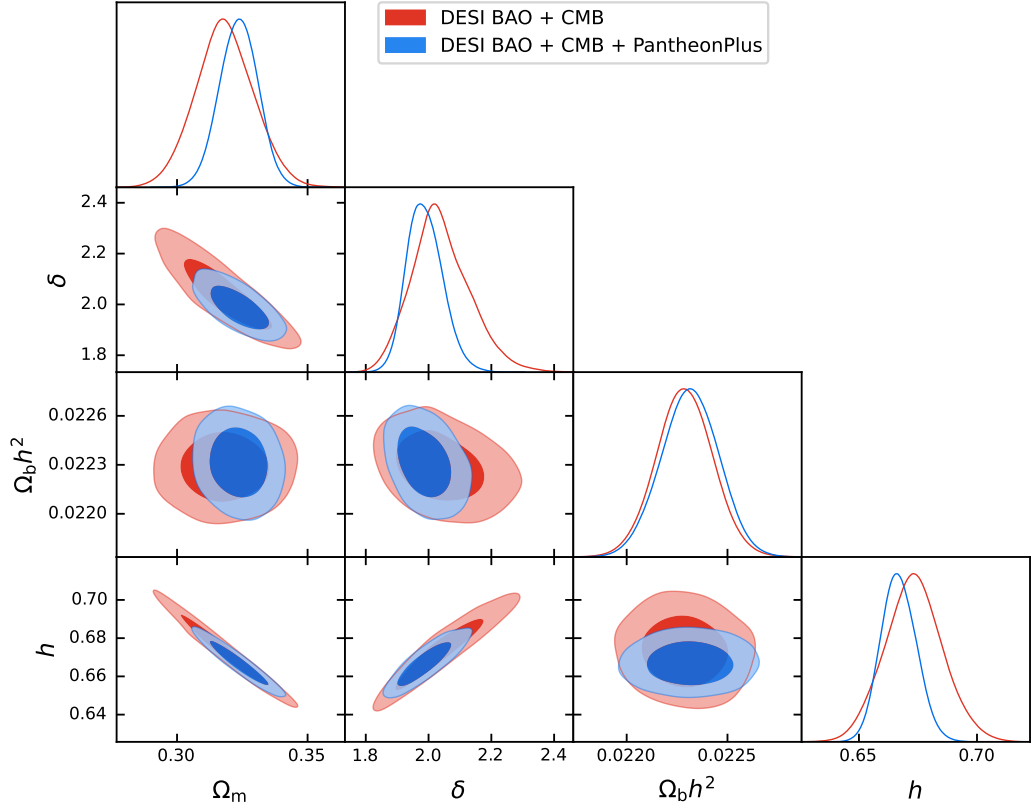


Figure 7. One-dimensional posterior distributions and two-dimensional marginalized contours at 1σ and 2σ levels for THDE model

spacetime structure and $\Delta = 1$ representing the most intricate deformation. By applying Barrow entropy to UV/IR relation, E. N. Saridakis proposed the Barrow HDE (BHDE) model [70]. In this model, the HDE density is modified as

$$\rho_{de} = BL^{\Delta-2}. \quad (3.34)$$

In the BHDE model, the future event horizon serves as the IR cutoff. The Friedmann equation also satisfies Eq. (3.32), and the evolution equation for Ω_{de} is [101]

$$\begin{aligned} \frac{d\Omega_{de}}{dz} = & -\frac{\Omega_{de}(1-\Omega_{de})}{1+z} \left[\left(1 + \frac{\Delta}{2}\right) \mathcal{F}_r + (\Delta+1) \mathcal{F}_m \right. \\ & \left. + G(1-\Omega_{de})^{\frac{\Delta}{2(\Delta-2)}} (\Omega_{de})^{\frac{1}{2-\Delta}} \right], \end{aligned} \quad (3.35)$$

where

$$\begin{aligned} \mathcal{F}_r &= \frac{2\Omega_r(1+z)^4}{\Omega_m(1+z)^3 + \Omega_r(1+z)^4}, \\ \mathcal{F}_m &= \frac{\Omega_m(1+z)^3}{\Omega_m(1+z)^3 + \Omega_r(1+z)^4}, \\ G &\equiv (2-\Delta) \left(\frac{B}{3M_P^2} \right)^{\frac{1}{\Delta-2}} (H_0 \sqrt{\Omega_m(1+z)^3 + \Omega_r(1+z)^4})^{\frac{\Delta}{2-\Delta}}. \end{aligned} \quad (3.36)$$

Model	DESI BAO+CMB		
	χ^2_{\min}	$\ln \mathcal{B}_{12}$	Rank
ΛCDM	21.22	0	1
OHDE	21.61	-2.18	2
THDE	21.20	-2.39	2
BHDE	20.86	-3.34	2
GRDE	16.87	-5.80	2
IHDE2	22.55	-9.55	3
IHDE1	40.45	-13.74	3
RDE	183.70	-89.61	4

Table 4. The χ^2 statistic values and relative Bayesian evidence for each model in BAO+CMB dataset. The models follow the relative Bayesian evidence in descending order.

The EoS is given by

$$w = -\frac{1+\Delta}{3} - \frac{G}{3}(\Omega_{de})^{\frac{1}{2-\Delta}}(1-\Omega_{de})^{\frac{\Delta}{2(\Delta-2)}}e^{\frac{3\Delta}{2(2-\Delta)}x}. \quad (3.37)$$

For consistency with the THDE, we fixed $B = 3$ in M_P^2 units to perform constraints. When $\Delta = 0$, this model reduces to the OHDE scenario.

Fig. 8 presents the one-dimensional posterior distributions and two-dimensional marginalized contours of combined observational constraints for the BHDE model. The overall constraint patterns show similarities to those observed in the OHDE and IHDE2 models, both of which use the future event horizon as a cutoff. While the BAO+CMB (red) data provides a broad constraint, the inclusion of PantheonPlus data (blue) generally tightens the parameter constraints, particularly for Ω_m , Δ , and h . The blue contours favor higher value of Ω_m , and lower values of Δ , and h . In addition, there is a noticeable discrepancy between the results for the blue contours and those for the red contours.

The best-fit values derived from the sample likelihood constraints are listed in Table 3. For the BAO+CMB dataset, the best-fit values with 1σ CL are $\Omega_m = 0.2921^{+0.0321}_{-0.0338}$, $h = 0.7000^{+0.0459}_{-0.0361}$, and $\Delta = 0.2349^{+0.0740}_{-0.0724}$, which yields an EoS of $w = -1.26^{+0.11}_{-0.18}$ at $z = 0$. In the BAO+CMB+SN dataset, we have $\Omega_m = 0.3261^{+0.0157}_{-0.0137}$, $h = 0.6606^{+0.0130}_{-0.0147}$, and $\Delta = 0.1581^{+0.0298}_{-0.0379}$, resulting in $w = -1.09^{+0.04}_{-0.04}$ at $z = 0$. Based on the parameter constrain results given by the two datasets, the discrepancies for Ω_m , Δ , and h are 0.94σ , 0.95σ , and 0.91σ , respectively.

Both datasets yield a EoS of BHDE $w < -1$, indicating that BHDE also have phantom-like characteristics. Similar to the OHDE models, the EoS of the BHDE model deviates significantly from the Λ CDM case ($w = -1$) when only the BAO+CMB data are considered. However, the inclusion of the SN data leads to the EoS of BHDE much closer to the cosmological constant. Again, this implies that under the framework of HDE with future event horizon as the IR cutoff, the PantheonPlus dataset does not favor a dynamical DE.

4 Conclusion

The results of χ^2 statistic and Bayesian evidence for the two datasets are summarized in Table 4 and Table 5, respectively.

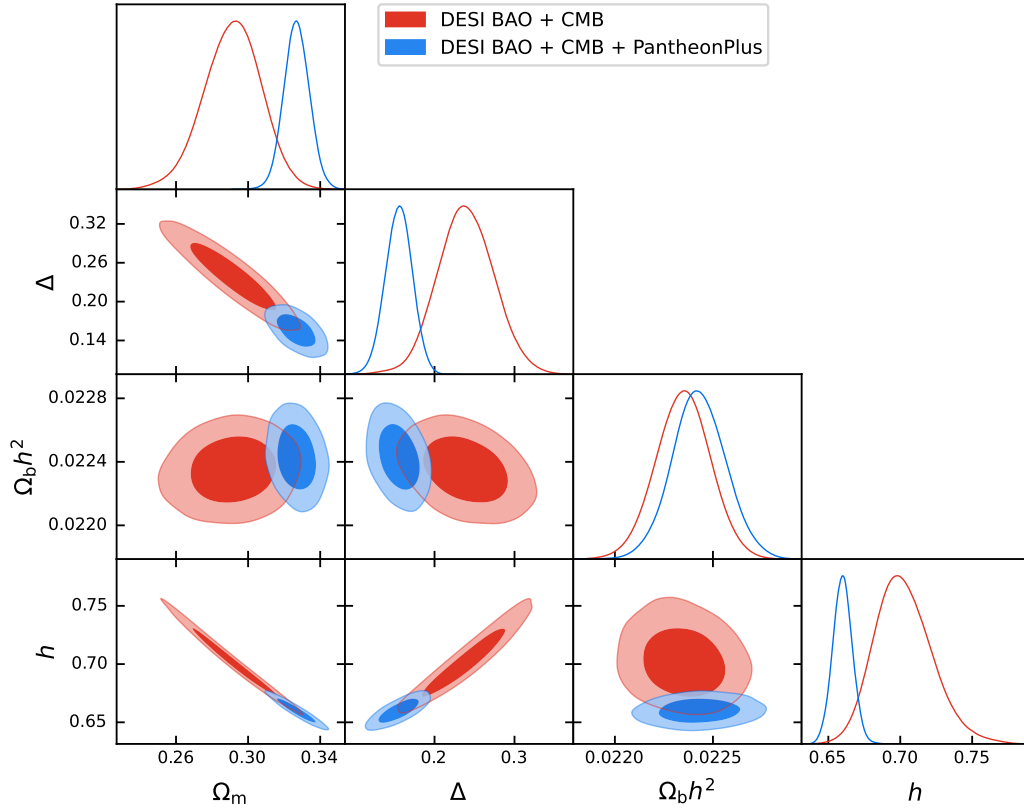


Figure 8. One-dimensional posterior distributions and two-dimensional marginalized contours at 1σ and 2σ levels for BHDE model

Model	DESI BAO+CMB+PantheonPlus		
	χ^2_{\min}	$\ln \mathcal{B}_{12}$	Rank
Λ CDM	1424.43	0	1
THDE	1424.28	-3.29	2
BHDE	1431.62	-7.61	2
GRDE	1422.87	-8.35	2
OHDE	1436.45	-9.78	2
IHDE2	1435.45	-15.15	3
IHDE1	1452.89	-18.81	3
RDE	1997.47	-291.46	4

Table 5. The χ^2 statistic values and relative Bayesian evidence for each model in BAO+CMB+PantheonPlus dataset. The models follow the relative Bayesian evidence in descending order.

Based on Bayesian evidence, we make a rank for all the DE models considered in this paper. For the case of the BAO+CMB dataset, the Λ CDM is in the first rank since it yields the best Bayesian evidence among all models. The OHDE, THDE, BHDE, and GRDE are classified in the second rank, with their Bayesian evidence greater than -6 . The IHDE2 and IHDE1 are placed in the third rank. Finally, the RDE, with the highest χ^2 values and the

lowest Bayesian evidence, is positioned in the fourth rank.

Different from the results of the BAO+CMB dataset, minor changes appear for the case of the BAO+CMB+SN dataset. The Λ CDM remains in the first rank. However, the order of the models in the second rank becomes: THDE, BHDE, GRDE and OHDE, with their Bayesian evidence greater than -10 . Due to the low Bayesian evidence, the IHDE2 and IHDE1 are still classified into the third rank. The RDE, which is ruled out by observation, is placed in the fourth rank.

Moreover, we draw the following key conclusions:

1. Based on Bayesian evidence, the Λ CDM remains the most competitive model, while the RDE model is ruled out by observational data.

2. HDE models with dark sector interaction perform the worst across all categories, indicating that the interaction term is not favored within the HDE framework.

3. The remaining three categories show relatively comparable performance. Specifically, the OHDE model has better performance in the BAO+CMB dataset, while the HDE models with modified black hole entropy outperforms other three categories in the BAO+CMB+SN dataset.

4. HDE models with the future event horizon as the IR cutoff exhibit significant discrepancies in parameter constraints between the BAO+CMB and BAO+CMB+PantheonPlus datasets. The BAO+CMB dataset favors a phantom-like DE, whereas the inclusion of PantheonPlus data brings the EoS much closer to the cosmological constant. This indicates that, in the framework of HDE with the future event horizon, the PantheonPlus dataset does not favor a dynamical DE.

5 Summary

In this paper, we perform the most comprehensive numerical study on all four categories of HDE. Seven representative HDE models across four categories are selected, including OHDE, RDE, GRDE, IHDE1, IHDE2, THDE, and BHDE. Among these models, the GRDE and IHDE2 introduce two additional free parameters compared to the Λ CDM, while the remaining models introduced only one additional parameter. For comparison, we adopt the Λ CDM model as the fiducial model. The observational data include DESI BAO 2024 measurements, Planck 2018 CMB distance priors, and the PantheonPlus compilation of SN. These data are divided into two sets: DESI BAO+CMB, and DESI BAO+CMB+PantheonPlus. We apply χ^2 statistic to evaluate the models' compatibility with current observational data, and then compare their relative performances with Bayesian evidence.

Based on Bayesian evidence, we find that these seven HDE models can be classified into four rank. The Λ CDM model is in the first rank, the OHDE, THDE, BHDE, and GRDE models are in the second rank, the IHDE2 and IHDE1 models are in the third rank, and the RDE is in the forth rank.

In addition, the inclusion of SN data introduces discrepancies in the performance of different HDE models. For the HDE models that adopt the Hubble scale as a IR cutoff, their EoS are very close to the cosmological constant, and the inclusion of PantheonPlus dataset does not affect the results. For HDE models that adopt the extended Hubble scale as a IR cutoff, their EoS exhibit phantom-like characteristics, and the inclusion of PantheonPlus dataset leads to slight discrepancies in the parameter constraints, thus bringing the EoS closer to -1 . Finally, for the HDE models that adopt the future event horizon as a cutoff,

their EoS display obvious phantom-like characteristics, and the inclusion of PantheonPlus dataset significantly alters parameters constraints, also bringing the EoS closer to -1 .

Our studies imply that, under the framework of HDE with future event horizon, the PantheonPlus dataset does not favor a dynamical DE. This indicates the importance of further investigating PantheonPlus SN data. It is interesting to explore the details of PantheonPlus SN samples, and then identify which redshift range plays a more important role in favoring the cosmological constant. Furthermore, instead of focusing on a specific class of DE models, one can also adopt model-independent methods to analyze observational data. These topics are worth further explorations in future works.

Acknowledgments

J.X. Li wants to thank Yi Zheng for helpful discussions about DESI BAO data. S.Wang is supported by a grant of Guangdong Provincial Department of Science and Technology under No. 2020A1414040009.

References

- [1] SUPERNOVA SEARCH TEAM collaboration, *Observational evidence from supernovae for an accelerating universe and a cosmological constant*, *Astron. J.* **116** (1998) 1009 [[astro-ph/9805201](#)].
- [2] SUPERNOVA COSMOLOGY PROJECT collaboration, *Measurements of Ω and Λ from 42 High Redshift Supernovae*, *Astrophys. J.* **517** (1999) 565 [[astro-ph/9812133](#)].
- [3] S. Weinberg, *The Cosmological Constant Problem*, *Rev. Mod. Phys.* **61** (1989) 1.
- [4] S.M. Carroll, *The Cosmological constant*, *Living Rev. Rel.* **4** (2001) 1 [[astro-ph/0004075](#)].
- [5] P.J.E. Peebles and B. Ratra, *The Cosmological Constant and Dark Energy*, *Rev. Mod. Phys.* **75** (2003) 559 [[astro-ph/0207347](#)].
- [6] T. Padmanabhan, *Cosmological constant: The Weight of the vacuum*, *Phys. Rept.* **380** (2003) 235 [[hep-th/0212290](#)].
- [7] E.J. Copeland, M. Sami and S. Tsujikawa, *Dynamics of dark energy*, *Int. J. Mod. Phys. D* **15** (2006) 1753 [[hep-th/0603057](#)].
- [8] J. Frieman, M. Turner and D. Huterer, *Dark Energy and the Accelerating Universe*, *Ann. Rev. Astron. Astrophys.* **46** (2008) 385 [[0803.0982](#)].
- [9] A. Silvestri and M. Trodden, *Approaches to Understanding Cosmic Acceleration*, *Rept. Prog. Phys.* **72** (2009) 096901 [[0904.0024](#)].
- [10] M. Li, X.-D. Li, S. Wang and Y. Wang, *Dark Energy*, *Commun. Theor. Phys.* **56** (2011) 525 [[1103.5870](#)].
- [11] K. Bamba, S. Capozziello, S. Nojiri and S.D. Odintsov, *Dark energy cosmology: the equivalent description via different theoretical models and cosmography tests*, *Astrophys. Space Sci.* **342** (2012) 155 [[1205.3421](#)].
- [12] M. Li, X.-D. Li, S. Wang and Y. Wang, *Dark Energy: A Brief Review*, *Front. Phys. (Beijing)* **8** (2013) 828 [[1209.0922](#)].
- [13] P. Bull et al., *Beyond Λ CDM: Problems, solutions, and the road ahead*, *Phys. Dark Univ.* **12** (2016) 56 [[1512.05356](#)].
- [14] J.S. Bullock and M. Boylan-Kolchin, *Small-Scale Challenges to the Λ CDM Paradigm*, *Ann. Rev. Astron. Astrophys.* **55** (2017) 343 [[1707.04256](#)].
- [15] A. Filippi and M. De Napoli, *Searching in the dark: the hunt for the dark photon*, *Rev. Phys.* **5** (2020) 100042 [[2006.04640](#)].
- [16] J. Sola Peracaula, *The cosmological constant problem and running vacuum in the expanding universe*, *Phil. Trans. Roy. Soc. Lond. A* **380** (2022) 20210182 [[2203.13757](#)].
- [17] L. Verde, T. Treu and A.G. Riess, *Tensions between the Early and the Late Universe*, *Nature Astron.* **3** (2019) 891 [[1907.10625](#)].
- [18] L. Perivolaropoulos and F. Skara, *Challenges for Λ CDM: An update*, *New Astron. Rev.* **95** (2022) 101659 [[2105.05208](#)].
- [19] N. Schöneberg, G. Franco Abellán, A. Pérez Sánchez, S.J. Witte, V. Poulin and J. Lesgourgues, *The H_0 Olympics: A fair ranking of proposed models*, *Phys. Rept.* **984** (2022) 1 [[2107.10291](#)].
- [20] E. Di Valentino, O. Mena, S. Pan, L. Visinelli, W. Yang, A. Melchiorri et al., *In the realm of the Hubble tension—a review of solutions*, *Class. Quant. Grav.* **38** (2021) 153001 [[2103.01183](#)].

- [21] E. Abdalla et al., *Cosmology intertwined: A review of the particle physics, astrophysics, and cosmology associated with the cosmological tensions and anomalies*, *JHEAp* **34** (2022) 49 [[2203.06142](#)].
- [22] M. Kamionkowski and A.G. Riess, *The Hubble Tension and Early Dark Energy*, *Ann. Rev. Nucl. Part. Sci.* **73** (2023) 153 [[2211.04492](#)].
- [23] V. Poulin, T.L. Smith and T. Karwal, *The Ups and Downs of Early Dark Energy solutions to the Hubble tension: A review of models, hints and constraints circa 2023*, *Phys. Dark Univ.* **42** (2023) 101348 [[2302.09032](#)].
- [24] C. Rong-Gen, L. Li and W. Shao-Jiang, *Hubble-constant crisis*, *Acta Phys. Sin.* **72** (2023) 239801.
- [25] G. Efstathiou, *Challenges to the Lambda CDM Cosmology*, 6, 2024 [[2406.12106](#)].
- [26] DESI collaboration, *DESI 2024 VI: Cosmological Constraints from the Measurements of Baryon Acoustic Oscillations*, [2404.03002](#).
- [27] M. Chevallier and D. Polarski, *Accelerating universes with scaling dark matter*, *Int. J. Mod. Phys. D* **10** (2001) 213 [[gr-qc/0009008](#)].
- [28] I.D. Gialamas, G. Hütsi, K. Kannike, A. Racioppi, M. Raidal, M. Vasar et al., *Interpreting DESI 2024 BAO: late-time dynamical dark energy or a local effect?*, [2406.07533](#).
- [29] S. Dhawan, B. Popovic and A. Goobar, *The axis of systematic bias in SN^{Ia} cosmology and implications for DESI 2024 results*, [2409.18668](#).
- [30] C. Wetterich, *Cosmology and the Fate of Dilatation Symmetry*, *Nucl. Phys. B* **302** (1988) 668 [[1711.03844](#)].
- [31] B. Ratra and P.J.E. Peebles, *Cosmological Consequences of a Rolling Homogeneous Scalar Field*, *Phys. Rev. D* **37** (1988) 3406.
- [32] R.R. Caldwell, *A Phantom menace?*, *Phys. Lett. B* **545** (2002) 23 [[astro-ph/9908168](#)].
- [33] T. Chiba, T. Okabe and M. Yamaguchi, *Kinetically driven quintessence*, *Phys. Rev. D* **62** (2000) 023511 [[astro-ph/9912463](#)].
- [34] C. Armendariz-Picon, V.F. Mukhanov and P.J. Steinhardt, *A Dynamical solution to the problem of a small cosmological constant and late time cosmic acceleration*, *Phys. Rev. Lett.* **85** (2000) 4438 [[astro-ph/0004134](#)].
- [35] C. Armendariz-Picon, V.F. Mukhanov and P.J. Steinhardt, *Essentials of k essence*, *Phys. Rev. D* **63** (2001) 103510 [[astro-ph/0006373](#)].
- [36] A.Y. Kamenshchik, U. Moschella and V. Pasquier, *An Alternative to quintessence*, *Phys. Lett. B* **511** (2001) 265 [[gr-qc/0103004](#)].
- [37] N. Bilic, G.B. Tupper and R.D. Viollier, *Unification of dark matter and dark energy: The Inhomogeneous Chaplygin gas*, *Phys. Lett. B* **535** (2002) 17 [[astro-ph/0111325](#)].
- [38] M.C. Bento, O. Bertolami and A.A. Sen, *Generalized Chaplygin gas, accelerated expansion and dark energy matter unification*, *Phys. Rev. D* **66** (2002) 043507 [[gr-qc/0202064](#)].
- [39] J. Yoo and Y. Watanabe, *Theoretical Models of Dark Energy*, *Int. J. Mod. Phys. D* **21** (2012) 1230002 [[1212.4726](#)].
- [40] S. Tsujikawa, *Quintessence: A Review*, *Class. Quant. Grav.* **30** (2013) 214003 [[1304.1961](#)].
- [41] A. Joyce, L. Lombriser and F. Schmidt, *Dark Energy Versus Modified Gravity*, *Ann. Rev. Nucl. Part. Sci.* **66** (2016) 95 [[1601.06133](#)].
- [42] K. Arun, S.B. Gudennavar and C. Sivaram, *Dark matter, dark energy, and alternate models: A review*, *Adv. Space Res.* **60** (2017) 166 [[1704.06155](#)].

- [43] S. Bahamonde, C.G. Böhrer, S. Carloni, E.J. Copeland, W. Fang and N. Tamanini, *Dynamical systems applied to cosmology: dark energy and modified gravity*, *Phys. Rept.* **775-777** (2018) 1 [[1712.03107](#)].
- [44] R. Kase and S. Tsujikawa, *Dark energy in Horndeski theories after GW170817: A review*, *Int. J. Mod. Phys. D* **28** (2019) 1942005 [[1809.08735](#)].
- [45] O. Avsajanishvili, G.Y. Chitov, T. Kahniashvili, S. Mandal and L. Samushia, *Observational Constraints on Dynamical Dark Energy Models*, *Universe* **10** (2024) 122 [[2310.16911](#)].
- [46] G. 't Hooft, *Dimensional reduction in quantum gravity*, *Conf. Proc. C* **930308** (1993) 284 [[gr-qc/9310026](#)].
- [47] L. Susskind, *The World as a hologram*, *J. Math. Phys.* **36** (1995) 6377 [[hep-th/9409089](#)].
- [48] S. Wang, Y. Wang and M. Li, *Holographic Dark Energy*, *Phys. Rept.* **696** (2017) 1 [[1612.00345](#)].
- [49] P. Horava and D. Minic, *Probable values of the cosmological constant in a holographic theory*, *Phys. Rev. Lett.* **85** (2000) 1610 [[hep-th/0001145](#)].
- [50] S.D. Thomas, *Holography stabilizes the vacuum energy*, *Phys. Rev. Lett.* **89** (2002) 081301.
- [51] S.D.H. Hsu, *Entropy bounds and dark energy*, *Phys. Lett. B* **594** (2004) 13 [[hep-th/0403052](#)].
- [52] S. Wang and M. Li, *Theoretical aspects of holographic dark energy*, *Commun. Theor. Phys.* **75** (2023) 117401.
- [53] M. Li, *A Model of holographic dark energy*, *Phys. Lett. B* **603** (2004) 1 [[hep-th/0403127](#)].
- [54] B. Guberina, R. Horvat and H. Nikolic, *Generalized holographic dark energy and the IR cutoff problem*, *Phys. Rev. D* **72** (2005) 125011 [[astro-ph/0507666](#)].
- [55] R.-G. Cai, *A Dark Energy Model Characterized by the Age of the Universe*, *Phys. Lett. B* **657** (2007) 228 [[0707.4049](#)].
- [56] H. Wei and R.-G. Cai, *A New Model of Agegraphic Dark Energy*, *Phys. Lett. B* **660** (2008) 113 [[0708.0884](#)].
- [57] Z.-P. Huang and Y.-L. Wu, *Holographic Dark Energy Characterized by the Total Comoving Horizon and Insights to Cosmological Constant and Coincidence Problem*, *Phys. Rev. D* **85** (2012) 103007 [[1202.4228](#)].
- [58] S. Nojiri and S.D. Odintsov, *Unifying phantom inflation with late-time acceleration: Scalar phantom-non-phantom transition model and generalized holographic dark energy*, *Gen. Rel. Grav.* **38** (2006) 1285 [[hep-th/0506212](#)].
- [59] C. Gao, F. Wu, X. Chen and Y.-G. Shen, *A Holographic Dark Energy Model from Ricci Scalar Curvature*, *Phys. Rev. D* **79** (2009) 043511 [[0712.1394](#)].
- [60] L.N. Granda and A. Oliveros, *Infrared cut-off proposal for the Holographic density*, *Phys. Lett. B* **669** (2008) 275 [[0810.3149](#)].
- [61] Y. Gong and T. Li, *A Modified Holographic Dark Energy Model with Infrared Infinite Extra Dimension(s)*, *Phys. Lett. B* **683** (2010) 241 [[0907.0860](#)].
- [62] W. Zimdahl and D. Pavon, *Interacting holographic dark energy*, *Class. Quant. Grav.* **24** (2007) 5461 [[astro-ph/0606555](#)].
- [63] B. Wang, Y.-g. Gong and E. Abdalla, *Transition of the dark energy equation of state in an interacting holographic dark energy model*, *Phys. Lett. B* **624** (2005) 141 [[hep-th/0506069](#)].
- [64] M.R. Setare, *Interacting holographic dark energy model in non-flat universe*, *Phys. Lett. B* **642** (2006) 1 [[hep-th/0609069](#)].

- [65] L. Xu, *Holographic Dark Energy Model with Hubble Horizon as an IR Cut-off*, *JCAP* **09** (2009) 016 [[0907.1709](#)].
- [66] B. Wang, E. Abdalla, F. Atrio-Barandela and D. Pavon, *Dark Matter and Dark Energy Interactions: Theoretical Challenges, Cosmological Implications and Observational Signatures*, *Rept. Prog. Phys.* **79** (2016) 096901 [[1603.08299](#)].
- [67] M. Tavayef, A. Sheykhi, K. Bamba and H. Moradpour, *Tsallis Holographic Dark Energy*, *Phys. Lett. B* **781** (2018) 195 [[1804.02983](#)].
- [68] E.N. Saridakis, K. Bamba, R. Myrzakulov and F.K. Anagnostopoulos, *Holographic dark energy through Tsallis entropy*, *JCAP* **12** (2018) 012 [[1806.01301](#)].
- [69] R. D’Agostino, *Holographic dark energy from nonadditive entropy: cosmological perturbations and observational constraints*, *Phys. Rev. D* **99** (2019) 103524 [[1903.03836](#)].
- [70] E.N. Saridakis, *Barrow holographic dark energy*, *Phys. Rev. D* **102** (2020) 123525 [[2005.04115](#)].
- [71] S. Srivastava and U.K. Sharma, *Barrow holographic dark energy with Hubble horizon as IR cutoff*, *Int. J. Geom. Meth. Mod. Phys.* **18** (2021) 2150014 [[2010.09439](#)].
- [72] P. Adhikary, S. Das, S. Basilakos and E.N. Saridakis, *Barrow holographic dark energy in a nonflat universe*, *Phys. Rev. D* **104** (2021) 123519 [[2104.13118](#)].
- [73] N. Drepanou, A. Lymperis, E.N. Saridakis and K. Yesmakhanova, *Kaniadakis holographic dark energy and cosmology*, *Eur. Phys. J. C* **82** (2022) 449 [[2109.09181](#)].
- [74] Q.-G. Huang and Y.-G. Gong, *Supernova constraints on a holographic dark energy model*, *JCAP* **08** (2004) 006 [[astro-ph/0403590](#)].
- [75] H.-C. Kao, W.-L. Lee and F.-L. Lin, *CMB constraints on the holographic dark energy model*, *Phys. Rev. D* **71** (2005) 123518 [[astro-ph/0501487](#)].
- [76] C. Feng, B. Wang, Y. Gong and R.-K. Su, *Testing the viability of the interacting holographic dark energy model by using combined observational constraints*, *JCAP* **09** (2007) 005 [[0706.4033](#)].
- [77] H.-b. Zhang, W. Zhong, Z.H. Zhu and S. He, *Exploring holographic dark energy model with Sandage-Leob test*, *Phys. Rev. D* **76** (2007) 123508 [[0705.4409](#)].
- [78] J. Lu, E.N. Saridakis, M.R. Setare and L. Xu, *Observational constraints on holographic dark energy with varying gravitational constant*, *JCAP* **03** (2010) 031 [[0912.0923](#)].
- [79] X. Zhang, *Holographic Ricci dark energy: Current observational constraints, quintom feature, and the reconstruction of scalar-field dark energy*, *Phys. Rev. D* **79** (2009) 103509 [[0901.2262](#)].
- [80] M. Li, X.-D. Li, S. Wang and X. Zhang, *Holographic dark energy models: A comparison from the latest observational data*, *JCAP* **06** (2009) 036 [[0904.0928](#)].
- [81] I. Duran, D. Pavon and W. Zimdahl, *Observational constraints on a holographic, interacting dark energy model*, *JCAP* **07** (2010) 018 [[1007.0390](#)].
- [82] Y. Wang and L. Xu, *Current Observational Constraints to Holographic Dark Energy Model with New Infrared cut-off via Markov Chain Monte Carlo Method*, *Phys. Rev. D* **81** (2010) 083523 [[1004.3340](#)].
- [83] M. Li, X. Li and X. Zhang, *Comparison of dark energy models: A perspective from the latest observational data*, *Sci. China Phys. Mech. Astron.* **53** (2010) 1631 [[0912.3988](#)].
- [84] T.-F. Fu, J.-F. Zhang, J.-Q. Chen and X. Zhang, *Holographic Ricci dark energy: Interacting model and cosmological constraints*, *Eur. Phys. J. C* **72** (2012) 1932 [[1112.2350](#)].

- [85] J.-F. Zhang, M.-M. Zhao, Y.-H. Li and X. Zhang, *Neutrinos in the holographic dark energy model: constraints from latest measurements of expansion history and growth of structure*, *JCAP* **04** (2015) 038 [[1502.04028](#)].
- [86] J. Cui, Y. Xu, J. Zhang and X. Zhang, *Strong gravitational lensing constraints on holographic dark energy*, *Sci. China Phys. Mech. Astron.* **58** (2015) 110402 [[1511.06956](#)].
- [87] Y.-Y. Xu and X. Zhang, *Comparison of dark energy models after Planck 2015*, *Eur. Phys. J. C* **76** (2016) 588 [[1607.06262](#)].
- [88] S. Wen, S. Wang and X. Luo, *Comparing dark energy models with current observational data*, *JCAP* **07** (2018) 011 [[1708.03143](#)].
- [89] S. Basilakos and S. Nesseris, *Conjoined constraints on modified gravity from the expansion history and cosmic growth*, *Phys. Rev. D* **96** (2017) 063517 [[1705.08797](#)].
- [90] X. Li, S.-P. Zhao, L. Tang and H.-N. Lin, *Holographic Dark Energy Model is Consistent with Pantheon SN Ia Data*, *Commun. Theor. Phys.* **71** (2019) 421.
- [91] W.J.C. da Silva and R. Silva, *Cosmological Perturbations in the Tsallis Holographic Dark Energy Scenarios*, *Eur. Phys. J. Plus* **136** (2021) 543 [[2011.09520](#)].
- [92] W.-M. Dai, Y.-Z. Ma and H.-J. He, *Reconciling Hubble Constant Discrepancy from Holographic Dark Energy*, *Phys. Rev. D* **102** (2020) 121302 [[2003.03602](#)].
- [93] M.P. Dabrowski and V. Salzano, *Geometrical observational bounds on a fractal horizon holographic dark energy*, *Phys. Rev. D* **102** (2020) 064047 [[2009.08306](#)].
- [94] F.K. Anagnostopoulos, S. Basilakos and E.N. Saridakis, *Observational constraints on Barrow holographic dark energy*, *Eur. Phys. J. C* **80** (2020) 826 [[2005.10302](#)].
- [95] A. Hernández-Almada, G. Leon, J. Magaña, M.A. García-Aspeitia, V. Motta, E.N. Saridakis et al., *Kaniadakis-holographic dark energy: observational constraints and global dynamics*, *Mon. Not. Roy. Astron. Soc.* **511** (2022) 4147 [[2111.00558](#)].
- [96] X.-W. Qiu, Z.-W. Zhao, L.-F. Wang, J.-F. Zhang and X. Zhang, *A forecast of using fast radio burst observations to constrain holographic dark energy*, *JCAP* **02** (2022) 006 [[2108.04127](#)].
- [97] M. Rezaei and J. Sola Peracaula, *Running vacuum versus holographic dark energy: a cosmographic comparison*, *Eur. Phys. J. C* **82** (2022) 765 [[2207.14250](#)].
- [98] A. Oliveros, M.A. Sabogal and M.A. Acero, *Barrow holographic dark energy with Granda–Oliveros cutoff*, *Eur. Phys. J. Plus* **137** (2022) 783 [[2203.14464](#)].
- [99] G.G. Luciano, *Saez–Ballester gravity in Kantowski–Sachs Universe: A new reconstruction paradigm for Barrow Holographic Dark Energy*, *Phys. Dark Univ.* **41** (2023) 101237 [[2301.12488](#)].
- [100] W. Feng, W. Yang, B. Jiang, Y. Wang, T. Han and Y. Wu, *Theoretical analysis on the Barrow holographic dark energy in the Finsler–Randers cosmology*, *Int. J. Mod. Phys. D* **32** (2023) 2350029.
- [101] T. Denkiewicz, V. Salzano and M.P. Dabrowski, *Barrow nearly-extensive Gibbs-like entropy favored by dynamical and geometrical data sets in cosmology*, *Phys. Rev. D* **108** (2023) 103533 [[2303.11680](#)].
- [102] R. Nakarachinda, C. Pongkitivanichkul, D. Samart, L. Tannukij and P. Wongjun, *Rényi Holographic Dark Energy*, *Fortsch. Phys.* **72** (2024) 2400073 [[2312.16901](#)].
- [103] W. Fang, G. Chen, C.-J. Feng, W. Du and C. Shu, *Acceleration of the Universe without the Hubble tension with Kaniadakis holographic dark energy using the Hubble horizon as the IR cut-off*, [2406.09209](#).
- [104] P. Adolf, M. Hirsch, S. Krieg, H. Päs and M. Tabet, *Fitting the DESI BAO data with dark energy driven by the Cohen–Kaplan–Nelson bound*, *JCAP* **08** (2024) 048 [[2406.09964](#)].

- [105] X. Tang, Y.-Z. Ma, W.-M. Dai and H.-J. He, *Constraining holographic dark energy and analyzing cosmological tensions*, *Phys. Dark Univ.* **46** (2024) 101568 [[2407.08427](#)].
- [106] T.-N. Li, Y.-H. Li, G.-H. Du, P.-J. Wu, L. Feng, J.-F. Zhang et al., *Revisiting holographic dark energy after DESI 2024*, [2411.08639](#).
- [107] U.K. Tyagi, S. Haridasu and S. Basak, *Holographic and gravity-thermodynamic approaches in entropic cosmology: Bayesian assessment using late-time data*, *Phys. Rev. D* **110** (2024) 063503 [[2406.07446](#)].
- [108] C. Hahn et al., *The DESI Bright Galaxy Survey: Final Target Selection, Design, and Validation*, *Astron. J.* **165** (2023) 253 [[2208.08512](#)].
- [109] DESI collaboration, *Target Selection and Validation of DESI Luminous Red Galaxies*, *Astron. J.* **165** (2023) 58 [[2208.08515](#)].
- [110] A. Raichoor et al., *Target Selection and Validation of DESI Emission Line Galaxies*, *Astron. J.* **165** (2023) 126 [[2208.08513](#)].
- [111] E. Chaussidon et al., *Target Selection and Validation of DESI Quasars*, *Astrophys. J.* **944** (2023) 107 [[2208.08511](#)].
- [112] D.J. Eisenstein and W. Hu, *Baryonic features in the matter transfer function*, *Astrophys. J.* **496** (1998) 605 [[astro-ph/9709112](#)].
- [113] G. Strang, *Introduction to linear algebra*, Wellesley Cambridge Press, Wellesley, MA (2000).
- [114] PLANCK collaboration, *Planck 2018 results. VI. Cosmological parameters*, *Astron. Astrophys.* **641** (2020) A6 [[1807.06209](#)].
- [115] G. Efstathiou and J.R. Bond, *Cosmic confusion: Degeneracies among cosmological parameters derived from measurements of microwave background anisotropies*, *Mon. Not. Roy. Astron. Soc.* **304** (1999) 75 [[astro-ph/9807103](#)].
- [116] Y. Wang and P. Mukherjee, *Robust dark energy constraints from supernovae, galaxy clustering, and three-year wilkinson microwave anisotropy probe observations*, *Astrophys. J.* **650** (2006) 1 [[astro-ph/0604051](#)].
- [117] Y. Wang and P. Mukherjee, *Observational Constraints on Dark Energy and Cosmic Curvature*, *Phys. Rev. D* **76** (2007) 103533 [[astro-ph/0703780](#)].
- [118] L. Chen, Q.-G. Huang and K. Wang, *Distance Priors from Planck Final Release*, *JCAP* **02** (2019) 028 [[1808.05724](#)].
- [119] Z. Zhai, C.-G. Park, Y. Wang and B. Ratra, *CMB distance priors revisited: effects of dark energy dynamics, spatial curvature, primordial power spectrum, and neutrino parameters*, *JCAP* **07** (2020) 009 [[1912.04921](#)].
- [120] W. Hu and N. Sugiyama, *Small scale cosmological perturbations: An Analytic approach*, *Astrophys. J.* **471** (1996) 542 [[astro-ph/9510117](#)].
- [121] Z. Zhai and Y. Wang, *Robust and model-independent cosmological constraints from distance measurements*, *JCAP* **07** (2019) 005 [[1811.07425](#)].
- [122] D. Brout et al., *The Pantheon+ Analysis: Cosmological Constraints*, *Astrophys. J.* **938** (2022) 110 [[2202.04077](#)].
- [123] J. Torrado and A. Lewis, *Cobaya: Code for Bayesian Analysis of hierarchical physical models*, *JCAP* **05** (2021) 057 [[2005.05290](#)].
- [124] A. Lewis, *Efficient sampling of fast and slow cosmological parameters*, *Phys. Rev. D* **87** (2013) 103529 [[1304.4473](#)].
- [125] A. Lewis and S. Bridle, *Cosmological parameters from CMB and other data: A Monte Carlo approach*, *Phys. Rev. D* **66** (2002) 103511 [[astro-ph/0205436](#)].

- [126] A. Gelman and D.B. Rubin, *Inference from Iterative Simulation Using Multiple Sequences*, *Statist. Sci.* **7** (1992) 457.
- [127] A. Lewis, *GetDist: a Python package for analysing Monte Carlo samples*, [1910.13970](#).
- [128] W.J. Handley, M.P. Hobson and A.N. Lasenby, *PolyChord: nested sampling for cosmology*, *Mon. Not. Roy. Astron. Soc.* **450** (2015) L61 [[1502.01856](#)].
- [129] W.J. Handley, M.P. Hobson and A.N. Lasenby, *polychord: next-generation nested sampling*, *Mon. Not. Roy. Astron. Soc.* **453** (2015) 4385 [[1506.00171](#)].
- [130] E.O. Colgáin and M.M. Sheikh-Jabbari, *A critique of holographic dark energy*, *Class. Quant. Grav.* **38** (2021) 177001 [[2102.09816](#)].
- [131] A. Aboubrahim and P. Nath, *Interacting ultralight dark matter and dark energy and fits to cosmological data in a field theory approach*, *JCAP* **09** (2024) 076 [[2406.19284](#)].
- [132] A. Aboubrahim and P. Nath, *Transmutation of interacting quintessence in the late universe*, [2411.11177](#).
- [133] D. Pavon and W. Zimdahl, *Holographic dark energy and cosmic coincidence*, *Phys. Lett. B* **628** (2005) 206 [[gr-qc/0505020](#)].
- [134] C. Tsallis and L.J.L. Cirto, *Black hole thermodynamical entropy*, *Eur. Phys. J. C* **73** (2013) 2487 [[1202.2154](#)].
- [135] J.D. Barrow, *The Area of a Rough Black Hole*, *Phys. Lett. B* **808** (2020) 135643 [[2004.09444](#)].
- [136] J.D. Barrow, S. Basilakos and E.N. Saridakis, *Big Bang Nucleosynthesis constraints on Barrow entropy*, *Phys. Lett. B* **815** (2021) 136134 [[2010.00986](#)].